Astron. Astrophys. 217, 157–178 (1989)

ASTRONOMY AND ASTROPHYSICS

OH maser emission from young planetary nebulae

Albert A. Zijlstra[1], Peter te Lintel Hekkert[2], Stuart R. Pottasch[1], J. L. Caswell[3], Mezak Ratag[1,4], and Harm J. Habing[2]

[1] Kapteyn Laboratorium, P.O. Box 800, NL–9700 AV Groningen, The Netherlands
[2] Sterrewacht Leiden, P.O. Box 9513, NL–2300 RA Leiden, The Netherlands
[3] CSIRO, Division of Radiophysics, P.O. Box 76, Epping, NSW, Australia
[4] Indonesia National Institute of Aeronautics and Space (LAPAN)

Received August 30, 1988; accepted February 14, 1989

Summary. OH emission, primarily in the 1612 MHz satellite line but also in the main lines, is detected in a number of young planetary nebulae. These objects form a direct observational link between the evolved OH/IR stars and planetary nebulae. In this paper we present the observations and discuss the implications for various aspects of Post–Asymptotic Giant Branch evolution. Life times and birth rates of this evolutionary stage are calculated. We propose a scheme for classifying pre-planetary nebula objects.

Key words: planetary nebulae – OH/IR stars – masers – evolution of stars

1. Introduction

One of the least understood phases of stellar evolution occurs at the tip of the Asymptotic Giant Branch (AGB) and immediately following the AGB. The envelope ejected during the AGB contains a large amount of dust, which completely obscures the central star. The visual extinction can be in excess of 100 magnitudes. Some time after the mass loss phase has ended the star becomes hot enough to ionize the nebula and the object emerges again as a planetary nebula. Only a few objects are known to be in the transition phase between the AGB and planetary nebula. Such objects are commonly called proto–planetary nebulae (PPN) or post-AGB stars; a recent compilation of nearby candidates can be found in Burrajabal et al. (1988). A review of observations concerning the post-AGB evolution can be found in Kwok (1986).

The stellar population at the tip of the AGB consists mainly of OH/IR stars and carbon stars, distinguished by an oxygen rich or a carbon rich envelope respectively. Both kinds of stars presumably evolve from Mira variables, and both can be progenitors of planetary nebulae (PN), though the details of the evolutionary process are not known. Oxygen rich stars are most easily detected, because their envelope can produce an OH maser line detectable throughout the galaxy. The maser line at 1612 MHz shows a characteristic double peaked shape, which is explained as arising in a spherical, uniformly expanding shell. Maximum amplification occurs along the line of sight through the center of the nebula, where the longest path length at a constant velocity is found. The blue shifted peak comes from the front of the nebula, the red shifted from the rear. Herman and Habing (1985), Habing et al. (1989) and Jones (1987) give recent reviews of observations of these OH/IR stars.

During the post-AGB evolution the objects are expected to go through a phase where the inner part of the envelope is already ionized while the outer regions are still neutral. If the envelope is oxygen rich, such an object could exhibit OH emission from the neutral region as well as radio continuum emission from the ionized gas, and would thus resemble both an OH/IR star and a planetary nebula. Until recently only one candidate for this phase was known, the compact planetary nebula Vy 2–2. The OH maser of Vy 2–2 was found by Davis (1979), and the nebula was studied further by Seaquist and Davis (1983). Extensive surveys to detect either radio continuum emission from OH/IR stars (Herman et al., 1985; Rodriguez et al., 1985a), or OH maser emission from PN, yielded only one more candidate: NGC 6302 (Payne et al., 1988), a bright and well-studied nebula.

Recently the IRAS satellite has opened a new window on PPN. Both young PN and OH/IR stars are strong far infrared emitters, because the absorbed stellar light is reradiated by the dust at infrared wavelengths. PPN appear to be readily identifiable in the IRAS point source catalogue (e.g. Olnon et al., 1984). The measured colour temperatures form a continuous sequence from about 800 K for the warmest OH/IR stars to about 80 K for the coldest PN (Pottasch et al., 1988; Chapman, 1987). This value refers to the average temperature of the dust, since the envelope contains a range of dust temperatures, being warmer closer to the central star (Phillips and Mampaso, 1988). Some OH/IR stars have colour temperatures within the range of PN, significantly colder than shown by ordinary OH/IR stars. They probably are in a phase where the mass loss has stopped and the envelope has become detached from the central star (Sun and Kwok, 1987). Depending on how fast the temperature of the central star is rising they are prime candidates to have entered the phase of OH emitting PN. The ionization must start within a few times 10^3 year after the massloss ends, otherwise the envelope will have dispersed and the OH emission stopped before the nebula becomes detectable in the radio continuum.

Send offprint requests to: A. A. Zijlstra

After the onset of ionization, the nebula is expected to be fully ionized within 10^3 yr (Spergel et al., 1983).

The IRAS database has resulted in the discovery of large numbers of OH/IR stars (te Lintel Hekkert et al., 1989b; te Lintel Hekkert et al., 1989c; Eder et al., 1988), as well as a group of PN which are in an earlier phase of evolution than had been observed before (Ratag et al., 1989; Pottasch et al., 1988). We have used these new samples to find more OH emitting PN. Firstly, selected OH/IR stars were observed in the radio continuum with the Very Large Array (VLA): preliminary results of this continuum survey have been published in Pottasch et al. (1987) and Zijlstra and Pottasch (1988). Secondly, a number of the newly found young PN were observed in the OH transitions using single-dish telescopes. Ten additional objects are found to exhibit both an OH maser line and radio continuum emission, bringing the total to twelve. These objects, called OHPN in the remainder of the paper, bridge the observational gap between the AGB and optically identifiable PN.

2. Sample selection and observations

In this paper we identify three different samples of possible PPN. The first sample (section (2.1) is a selection of OH/IR stars observed with the VLA for continuum emission. The presence of continuum, which is not normally seen in OH/IR stars, indicates that the inner envelope is already ionized and a planetary nebula has formed. The second sample (section 2.2) is obtained by searching for OH emission from the vicinity of known PN. We were able to find OH emission from a number of young PN, even though such emission has rarely been detected in the past. Finally, we have correlated existing catalogues of OH/IR stars and PN (section 2.3).

2.1. VLA survey of known OH/IR stars

2.1.1. Sample selection

The sample of 66 OH/IR stars is selected from "A catalogue of stellar 1612 MHz maser sources" (te Lintel Hekkert et al., 1989a; hereafter OH/IR star catalogue), which contains about 400 known OH/IR stars and close to 1400 new OH/IR sources discovered by follow-up observations of IRAS sources. Two selection criteria are used:

1. The 25 μm IRAS flux density, S_{25}, has to be greater than $1.25 \times S_{12}$, which defines an IRAS colour temperature within the range shown by young PN. This criterium selects against young OH/IR stars, since most of these have significantly higher colour temperatures.

2. The red shifted OH peak has to be weak or absent. This indicates that the ionization of the circumstellar envelope may have started. Because of the high densities in the inner envelope the ionized region will rapidly become optically thick at 18 cm, and thus the red shifted 1612 MHz line, which comes from the far side of the shell, will be affected by absorption.

Some objects which do not satisfy the second condition are still included in the sample.

2.1.2. VLA continuum observations

The 66 selected OH/IR stars were searched with the VLA of the National Radio Astronomy Observatory (NRAO) for continuum emission at a wavelength of 2 cm in September 1986 and April 1987. During the first observing run the VLA was in the B configuration, which gives a resolution of 1″ at 2 cm. The second observing run was carried out while the VLA was in D configuration with a resolution of roughly 6″. All observations were carried out with 3 minute on-source integration time. Although the receivers have a somewhat higher system temperature at 2 cm, this wavelength was chosen instead of 6 cm because (1) optically thick sources will have a higher flux density at 2 cm and (2) confusion with extragalactic sources is less of a problem. The flux calibration was done using 3C286, adopting a 2 cm flux density of 3.45 Jy. We estimate the error in the flux calibration to be less than 10%.

The positions of most OH/IR stars have only been measured with single dish radio telescopes, and generally are uncertain to several arcminutes. We used the positions of the associated IRAS sources, which are accurate to better than 60″. OH/IR stars are strong far infrared emitters and most fields show only one IRAS source within the error box with the right colours, so there is little doubt about the identification of the OH maser with the IRAS source.

All fields which showed radio continuum sources consistent with the IRAS position were reobserved at 6 cm, in order to eliminate the non-thermal background sources. In three cases we found a radio continuum source with a thermal spectrum within the error box of the IRAS position. A fourth star, OH24.8–0.0, which had a possible detection at 2 cm, could not be confirmed at 6 cm due to confusion from a nearby HII region. The complete list of all observed OH/IR stars is given in Table C1 in the appendix.

2.1.3. VLA OH line observations

The three stars with a 6 cm confirmation were subsequently observed at 1612 MHz (July 1987) and 1665 MHz (January 1987) in right circular polarization with the VLA, in order to determine the precise position of the OH maser emission (see also Table 1). Thirty two channels were used with a velocity resolution of 1.1 km/s. The rms noise per channel was approximately 35mJy/beam. All three sources were detected at the correct position, although the emission from OH 349.36–0.20 is weak and needs confirmation. OH 0.9+1.3 was detected at both

Table 1. Parameters of the 18 cm observations

Parkes 64 meter radiotelescope	
beam size	12′.5 × 12′.5
velocity range	−250. to 250. km s^{-1}
velocity resolution	0.9 km s^{-1}
rms	0.08 Jy
Nançay radiotelescope	
beam	3′.5 × 18′.
velocity range	−270. to 270. km s^{-1}
velocity resolution	0.8 km s^{-1}
rms	0.04 Jy
VLA	
synthesized beam	10″
velocity resolution	1.1 km s^{-1}
number of channels	31
rms	0.035 Jy

transitions; OH 349.36–0.20 was only detected at 1665 MHz . OH 349.36–0.20 emits about 90% of the 1612 MHz maser emission in the left circular polarization. The absolute flux calibration for the 1612 MHz of OH 0.9+1.3 is unknown, due to an error in the on-line application of the system temperature correction. All other amplitudes were calibrated using 3C286.

2.2. Sample from recent surveys at Parkes and at Nançay

2.2.1. Sample selection

Young PN show a large spread in IRAS colour temperatures which are not necessarily related to their ages (e.g. van der Veen, 1988), therefore the colour temperatures cannot be used to select the youngest objects. Instead we use the InfraRed Excess (IRE), which is defined as the ratio of the total observed far infrared flux density over the expected flux density (see appendix A). The IRE is a measure of the stellar temperature for young PN, as will be shown below. Recent VLA and WSRT observations have found PN with much higher IRE values than had been observed before (Pottasch et al., 1988; Zijlstra et al., 1989). From a total list of 16 PN with such large IRE (larger than 3), 14 were observed in the 1612 MHz OH line. All selected sources lie in the direction of the galactic bulge, since the VLA and WSRT surveys were limited to sources in this direction.

2.2.2. Observations

From the sample of PN with high IRE, 14 sources were observed at the 18 cm OH lines either at Parkes or at Nançay. During May 1987 and September 1988 we observed with the Parkes 64 meter radiotelescope, using a dual-channel cooled FET receiver (Table 1). The system temperature was typically 38 K. The calibration is relative to Hydra A (PKS 0915–118) assuming an 18 cm flux of 36 Jy (18 Jy in each sense of linear polarization). The 1024 channel autocorrelator was split into two bands of 512 channels each, measuring the two linear polarizations simultaneously. We observed the 1612 MHz satellite line of the OH radical using the total power technique. Owing to the use of new and not yet completely tested software, the absolute velocities are uncertain by as much as 1 km s^{-1} .

The observations in Nançay were carried out during December 1987 (Table 1). The 1612 MHz and 1667 MHz transitions were observed simultaneously by splitting the 1024 channel autocorrelator into four banks, each bank observing the left or right circular polarization of one of the frequencies. We used a frequency switching technique. Each bank observed the velocity range –13 to 280 km s^{-1} , after which the central frequency was switched to cover the "negative" velocity range. The ratio of flux to antenna temperature was taken to be 1.1 Jy/K.

All quoted velocities are with respect to the Local Standard of Rest.

The observations of the 1612 MHz transition were seriously hampered by interference caused by the GLONASS satellite system (see also Carter, 1986). We were ultimately able to obtain interference free data.

Seven sources were detected (six at Parkes (# 3, 5, 6, 7, 10 and 11 from table 2) and one, PK 356+2° 1, with the radiotelescope at Nançay). PK 356+2° 1 was also observed at 1667 MHz , but not detected with an estimated 3 σ upperlimit of 0.16 Jy. Some of these detections can possibly be attributed to confusing sources within the telescope beam; this problem is addressed below.

2.3. Correlations between OH and PN catalogues

2.3.1. OH observations of known PN

We have used preliminary results of the OH survey of IRAS sources to see whether any of the OH observations included in the beam a known planetary nebula. All OH/IR stars in the described in the literature were also included in the search. We selected from the survey all positions which had a known PN within the primary beam of the telescope. The PN positions were taken from the catalogue described by Acker (1983). The difference between the observed (IRAS) position and the planetary nebula position had to be less than one third of the HPBW of the telescope. In these cases a non-detection at the (IRAS) position corresponds to a meaningful non-detection of the planetary nebula as well. Table C2, in the Appendix, lists all PN for which we have upper limits on 1612 MHz maser emission. About half of the number of sources come from the present correlation; the remainder are taken from Payne et al. (1988).

In a few such cases 1612 MHz maser emission was detected from a position close to a planetary nebula. In these cases the OH emission is possibly associated with the planetary nebula instead of the IRAS source. Table C3 lists the IRAS sources for which 1612 MHz emission was detected close to a planetary nebula. In the cases where the velocity of the optical nebula is known, it differs by more than 50 km s^{-1} from the velocity of the 1612 MHz maser emission. Some of the PN (e.g. PK 358+3° 1 and PK 358+3° 3) are in highly confused areas in the sky: more than one OH/IR star was detected at the IRAS positions. High positional resolution measurements are needed to either prove or disprove the association between the PN in Table C3 and the OH emission.

2.3.2. Known OH sources near the new PN

The OH/IR catalogue was used in a similar way to find known OH sources near the recently found high IRE PN, which are not yet in the Acker catalog. Three sources were found, all from the survey described by Olnon et al. (1981). (The results of the Olnon et al. survey will be published in the OH/IR catalogue.) Two of these sources were also in the Parkes OH survey (section 2.2; # 5 and 7 in Table 2). A third source (OH 358.518+0.322, #8 in Table 2) coincided with a very weak source found by Ratag et al. (1989).

Olnon et al. carried out their survey using a rectangular grid in galactic coordinates. From the relative strength of an OH source at neighbouring grid positions they derived positions accurate to within 2′. The PN (VLA) positions are identical to the positions of the three OH sources within these errors.

3. Confusion

All of the presently discussed sources lie in the direction of the galactic bulge. Due to the strong concentration of OH/IR stars in this direction, confusion becomes an important problem for single-dish 1612 MHz OH observations. In this section we will try to quantify the expected detection rate due to confusion. We use the survey by te Lintel Hekkert et al. (1989b), which was carried out with the same observational parameters as the observations described in section 2.2.2 .

Table 2. The sample of OHPN stars: positions

#	Name	VLA continuum position				IRAS position		OH position				Ref.
		l	b	α	δ	α	δ	α	δ	$\Delta\alpha$	$\Delta\delta$	
1	NGC 6302 PK 349+1° 1 IRAS 17103–3702	349°.509	1°.056	$17^h10^m21^s.3$	−37°02′43″	$17^h10^m21^s.7$	−37°02′45″					1,3
2	OH 349.36–0.20 IRAS 17150–3754	349.351	−0.211	17 15 04.0	−37 54 54	17 15 04.2	−37 54 53	$17^h15^m04^s.0$	−37°54′53″	0.″6	10″	4,8,9,11
3	IRAS 17207–2856	357.396	3.971	17 20 44.7	−28 55 52	17 20 45.5	−28 56 48					9,11
4	PK 356+2° 1 IRAS 17221–3038	356.154	2.766	17 22 06.1	−30 38 05	17 22 05.9	−30 38 06					9,11
5	IRAS 17347–3139	356.801	−0.055	17 34 45.9	−31 39 11	17 34 46.5	−31 39 15					10,11
6	IRAS 17371–2747	0.326	1.565	17 37 11.8	−27 48 38	17 37 11.6	−27 47 38	17 37 08.4	−27 48 30	2.″6	43″	9,13
7	IRAS 17375–2759	0.210	1.406	17 37 29.4	−27 59 29	17 37 31.6	−27 59 35	17 37 26.7	−28 00 04	2.″0	40″	9,13
8	IRAS 17375–3000	358.509	0.326	17 37 32.6	−30 00 29	17 37 32.2	−30 00 36	17 37 34.8	−30 00 10	1.″9	25″	10,13
9	OH 0.9+1.3 IRAS 17393–2727	0.892	1.342	17 39 24.7	−27 27 02	17 39 23.8	−27 27 05	17 39 24.8	−27 27 03	0.″3	5″	4,9,11
10	IRAS 17443–2949	359.446	−0.840	17 44 23.8	−29 49 44	17 44 23.3	−29 49 56	17 44 23.3	−29 49 52	0.″06	1″	10,11
11	IRAS 17580–3111	359.796	−4.072	17 58 08.0	−31 10 27	17 58 05.2	−31 11 19					10,11
12	Vy 2 – 2 PK 45–2° 1 IRAS 19219+0947	45.498	−2.703	19 21 59.3	09 48 00	19 21 59.0	09 47 58					4,6,12

References used for the position information and continuum observations :

1: Payne et al. 1988; 3: Pottasch 1984; 4: Pottasch et al. 1987;
6: Seaquist and Davis 1983; 9: Pottasch et al. 1988; 10: Ratag et al. 1988; 12: Clegg and Walsh 1988

References used for the information on the OH data :

8: Caswell et al. 1983; 9: Pottasch et al. 1988; 11: this work; 13: Olnon et al. 1981

The detection probability of 1612 MHz maser emission from selected IRAS sources in this survey is approximately 50% in the region of the galactic bulge (within 15° of the galactic centre), and 33% in the galactic disk area outside the Bulge. Assuming there is no difference in the nature of the IRAS sources found in the bulge and the disk (for which there are no direct or indirect indications known to the authors), the difference in detection probability must be due to the higher density of OH sources in the bulge. So we estimate a confusion level in the galactic bulge of about 20%.

The survey of te Lintel Hekkert et al. (1989b) includes a number of known PN. Generally these are not expected to show OH 1612 MHz maser emission (e.g. Payne et al., 1988; Rodriguez et al., 1985a). The actual "detection" rate is approximately 20% in the galactic bulge, and less than 5% elsewhere. Attributing all these coincidences to confusion, which is also indicated by the large difference between the 1612 MHz velocity and the optical velocity of the PN in those cases where the velocity of PN is known (see also Table C3), we again expect a confusion level of 20%.

Note that the confusion level will depend upon position in the bulge, with the highest levels being found in the plane near the galactic centre. The derived number of 20% is an average for the bulge. In addition, the confusion level also depends on parameters like sensitivity, HPBW of the telescope and velocity coverage.

The actual detection rate in our sample of known PN (as mentioned in 2.2.2) is 7 out of 14. We expect that about three of these may be due to unrelated sources within the field of view.

This calculation does not take into account the fact that in a few cases the identification of the IRAS source with the radio continuum source might be wrong. Since the high IRE sources do not have known optical counterparts, their classificaton as PN is based on the detection of radio continuum emission. We have found one source where this classification turned out to be wrong, namely IRAS 17374–3013. The continuum source found by Pottasch et al. (1988) is identical to the pulsar PSR 1737-30 (Braun et al., 1989), while the IRAS source is offset from this position by 2′. We did find OH emission in the field as well, but the position as determined by Olnon et al. (1981) is a few arcminutes displaced both from the continuum and the IRAS source. We expect that most of the high IRE PN are correctly identified, but possibly not all. The problem can only be resolved by high-resolution OH observations, to determine the precise position of the OH maser emission.

4. Description of the detected sources

4.1. OHPN

We have found a total of ten new sources which, within our positional accuracy, show both radio continuum emission and OH 1612 MHz maser emission. We will call these objects OHPN. Two other terms are in use for objects in transition from AGB-star to planetary nebula: PPN and post-AGB star. Post-AGB star has been used for (super)giants with large circumstellar envelopes at high galactic latitude (Parthasarathy and Pottasch, 1986; Waelkens et al., 1987). The term is preferable to PPN when, as in these cases, it is not known for certain whether they will evolve into a visible planetary nebula. These objects may evolve too slowly to ever ionize the envelope. The term PPN, on the other hand, has been defined differently by various authors (for a review see Rodriguez, 1987). We define the term OHPN

as objects which show an OH maser line as well as detectable radio continuum emission. Because of the significant ionization they are a subset of the PN.

The sample of proposed candidates for PPN has increased significantly in recent years (e.g. Likkel et al., 1987). They show a wide range of observational characteristics. The core mass (related to the ZAMS mass of the progenitor) and the metal abundance of the stellar atmosphere are probably the main discriminators between the different types of PPN. The field would greatly benefit from a better classification scheme and terminology.

In Fig. 1 the OH spectra of all 12 likely OHPN, including Vy 2–2 and NGC 6302, are plotted. The relevant observational parameters are listed in Table 1. Table 2 and 3 list the observed properties for all sources. The individual sources are discussed in the following sections. In each case we comment on the positional accuracy of the IRAS, OH, and radio continuum measurements, and on the possibility that the inclusion of the object in the sample of OHPN is due to confusion.

4.2. OHPN 1 (NGC 6302)

The spectrum of NGC 6302 in Fig. 1 confirms the results of Payne et al. (1988). The absorption seen in the 1667 MHz line appears to be real. The 1612 MHz profile is highly irregular, showing many different components closely spaced in velocity, instead of the regular two-peaked spectrum of common OH/IR star. The OH emission is seen projected unto the ionized region.

4.3. OHPN 2 (OH 349.36–0.20)

In the recent literature there is some confusion about the name of this source, due to the erroneous galactic coordinates in Pottasch et al. (1987). We propose to use the name suggested by Caswell et al. (1981), who first observed the weak 1612 MHz emission. The peak flux density of the strongly circularly polarized emission ($\approx$ 80–90%) is about 0.6 Jy. The VLA observations detected 1665 MHz emssion within a few arcseconds of the position of the continuum source. Emission at 1667 MHz , shown in Fig. 1[d], was already reported by Caswell et al. (1981), although they did not publish a spectrum. The 1667 MHz is somewhat stronger than the 1612 MHz , and shows with a peak flux density of about 0.8 Jy. The main lines are not detectably (circularly) polarized, less than $\approx$ 10%. All lines show plateaus of emission, although not covering a large velocity range. Such plateaus can indicate that the emitting shell is thin, as opposed to the very thick envelopes of ordinary OH/IR stars. In such cases the maser emission is possibly unsaturated (Alcock et al., 1986).

4.4. OHPN 3 and 4 (IRAS 17207–2856 and PK 356+2° 1)

These two sources are the weakest 1612 MHz emittors in Table 3. Both sources show profiles not uncommon for OH/IR stars. OHPN 4 is the only source discovered at Nançay. No accurate positions are known for the OH masers. The IRAS position for OHPN 3 deviates about 1′ from the continuum position. Although this is a fairly large deviation, it is not unusual that IRAS sources in areas with high source densities, like the galactic bulge, have large uncertainties in their position. It is also possible that the IRAS point source reduction has missed the IR source associated with OHPN 3 in favour of the IRAS source we now quote. Confusion with unrelated OH/IR stars is a possibility for both these sources.

4.5. OHPN 5 (IRAS 17346–3139)

The 1612 MHz spectrum shows two groups of emission; one between –50 and 0 km s^{-1}, and the other near –125 km s^{-1}. Recent VLA observations of this object confirm that the OH emission at –125 km s^{-1} coincides with the continuum source (Likkel, te Lintel Hekkert and Zijlstra; preliminary result). The nature and position of the other emission lines is not (yet) clear from these observations.

4.6. OHPN 6 (IRAS 17371–2747)

This source shows a 1612 MHz spectrum with a flat-topped component(s), which is unusual for OH/IR stars. The IRAS position is about 1′ off from the continuum position. The same remark about the uncertainties in the IRAS position holds as given for OHPN 3. The OH position (given by Olnon et al., 1981) and the continuum position are in good agreement. The peak OH flux density of this source has not changed significantly since February 1975. The observations by Olnon et al. (1981) do not have enough sensitivity to allow for detailed comparison between the profiles.

4.7. OHPN 7 (IRAS 17375–2759)

The 1612 MHz profile resembles the blue shifted velocity peak of profiles of common OH/IR stars, similar to what is seen in Vy 2–2. Linear polarization is not detected. The positions for the OH emission (from Olnon et al., 1981), continuum, and IR are all consistent within the uncertainties. The peak flux density and general shape of the profile has not changed substantially since February 1975, when the Olnon et al. observations were carried out.

4.8. OHPN 8 (IRAS 17375–3000)

The 6 cm continuum source detected by Ratag et al. (1989) needs confirmation. The OH source found by Olnon et al. (1981) shows a typical, bright (> 1 Jy) OH/IR profile. The epoch of this measurement is June 1979. A second, unrelated, OH/IR star (OH 358.436+0.439) was also in the beam of the Bonn telescope. The position of the continuum emission and the IRAS position are in good agreement. The position of the OH emission is also in agreement with the continuum and IRAS position, within the uncertainties given by Olnon et al.

4.9. OHPN 9 (OH 0.9+1.3)

This source, discovered by Kerr and Bowers (1974), is probably one of the intrinsically strongest 1612 MHz emitters in the galaxy. The spectrum shows three, possibly four, separate peaks around –120 km s^{-1}. The VLA OH–line measurements, obtained in July 1987, show an excellent positional agreement with the continuum source. The absolute calibration of the VLA 1612 MHz profile is uncertain due to on–line computer problems during the observations. In February 1988 we obtained additional Nançay observations with the same parameters as described in section

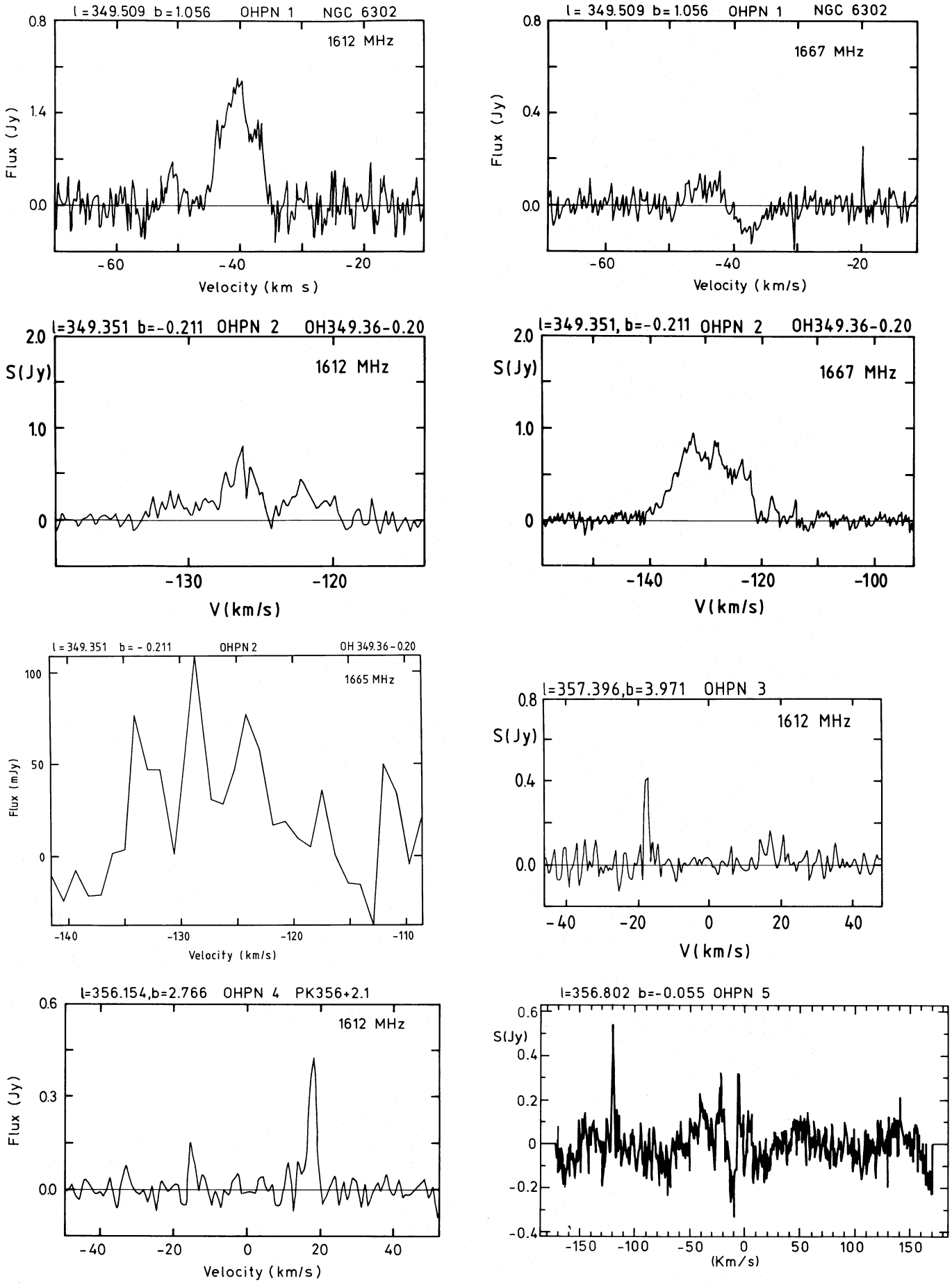

Fig. 1.

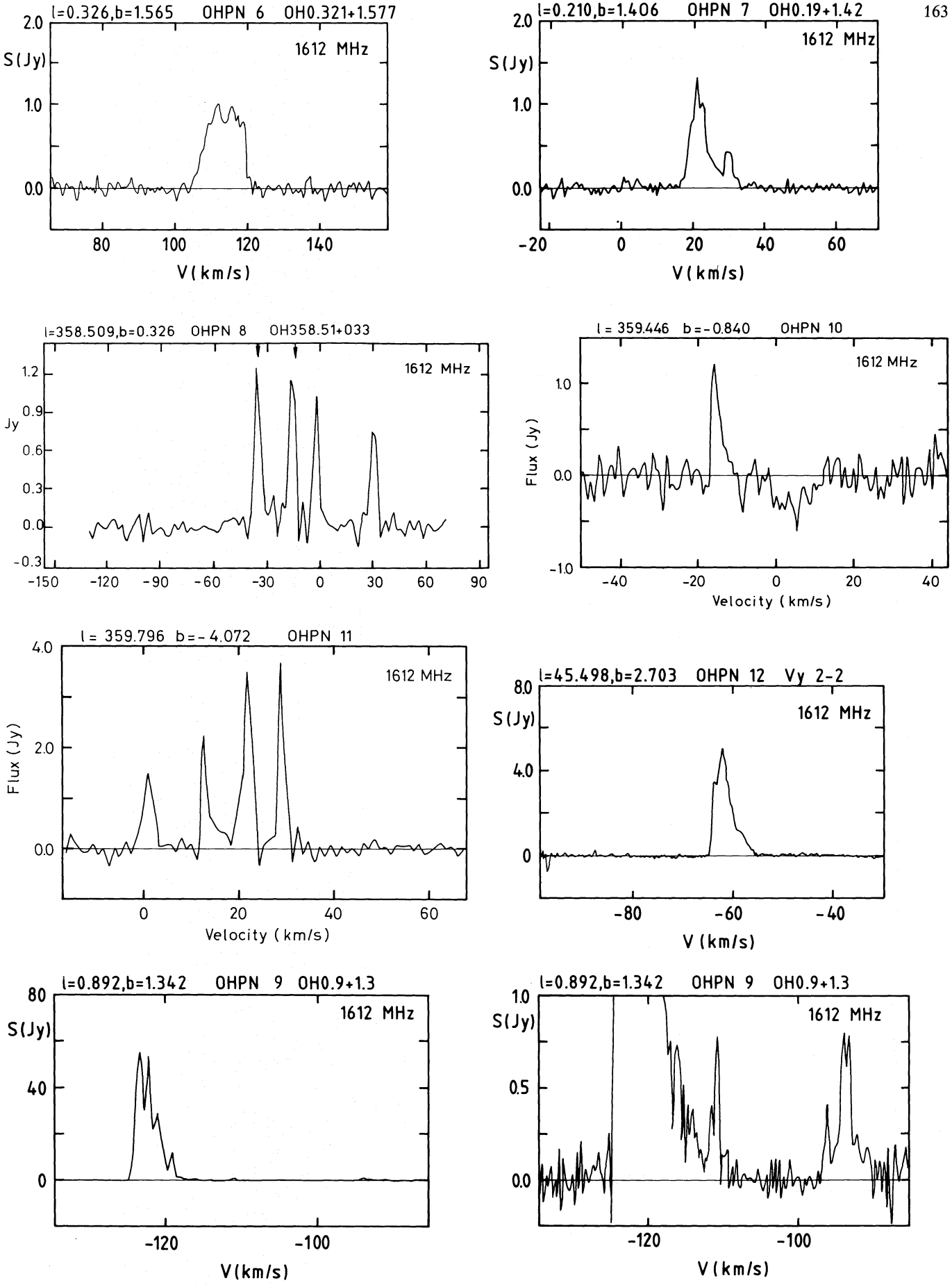

Fig. 1. (continued)

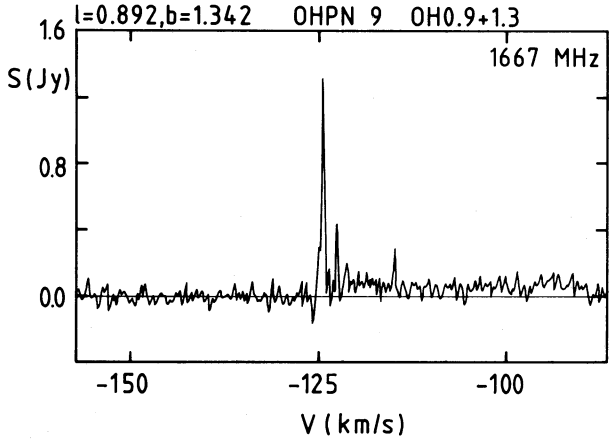

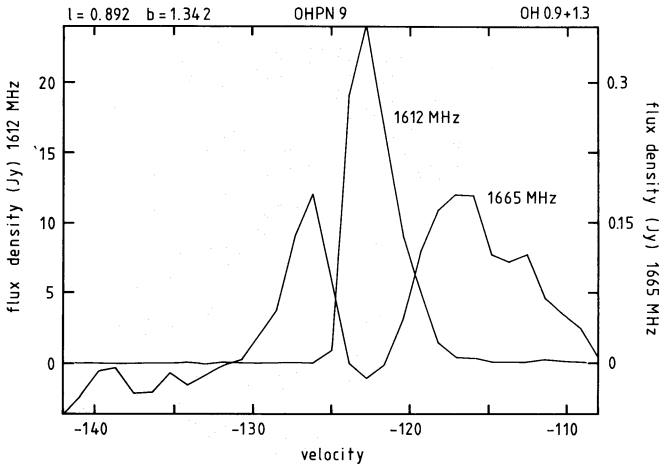

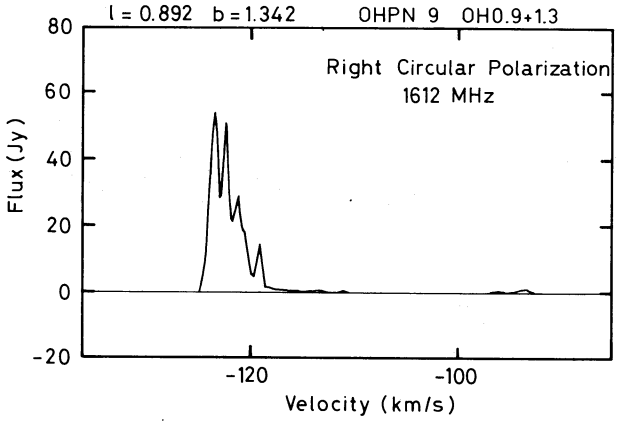

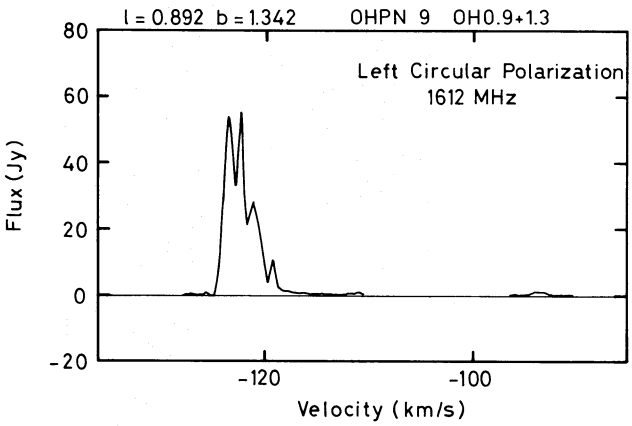

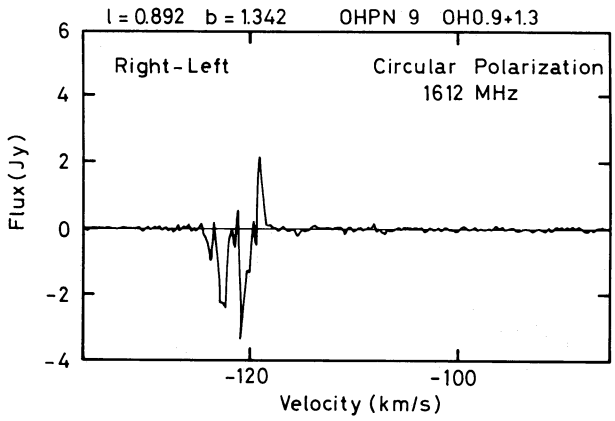

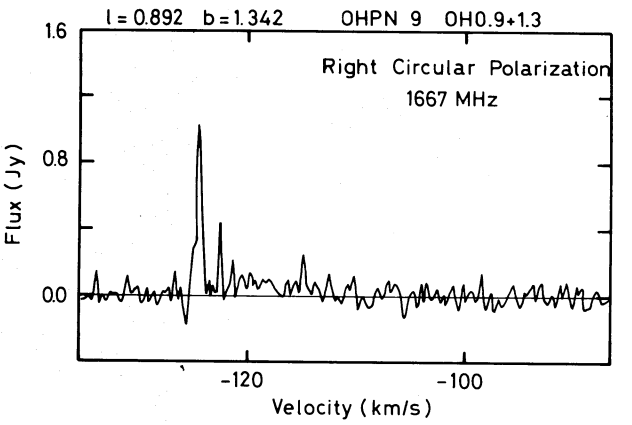

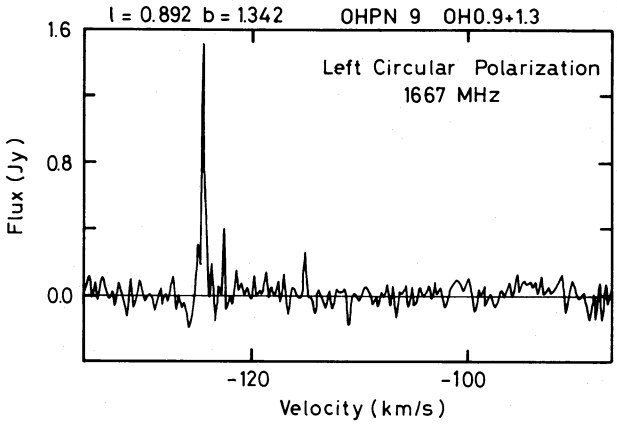

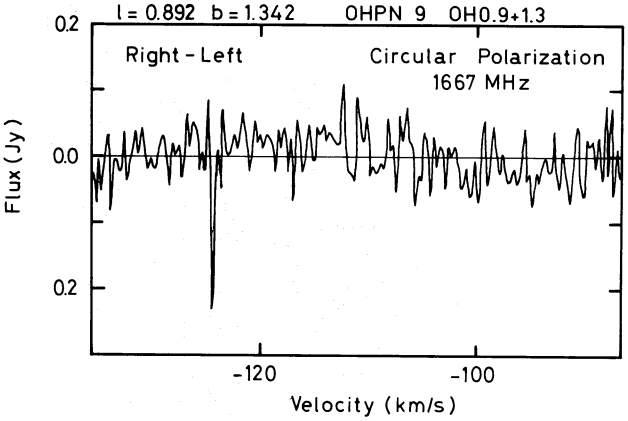

Fig. 1. (continued)

2.2.2; an additional (weak) component at –93.3 km s^{-1} was discovered. The maser spikes around –120 km s^{-1} are circularly polarized to about 15 %.

The spectrum has changed considerably since Kerr and Bowers first observed the source. Comparing the Nançay spectrum with the result from Kerr and Bowers shows that the two peaks at –123.5 and –122.3 km s^{-1} (the two outer most ones) have doubled in strength since 1974, as has the weak component at –116 km s^{-1}. The component at –121.2 km s^{-1} still shows the previous strength of 24 Jy.

A more detailed comparison between the right circular polarization measurement from Nançay and the VLA spectrum shows still larger differences between the spectra. The VLA spectrum does not show the spikes at –122.3, –121.2 and at –119.1 km s^{-1}. A 1612 MHz spectrum (although the observed position is off by 6′) obtained with the Parkes telescope in November 1985 shows a profile shape similar to the July 1987 VLA result. Therefore the change occurred between July 1987 and January 1988. During this time the three spikes regained their previous strength from 1974. We conclude that the source is variable on time scales as short as months. Unlike OH/IR stars, parts of the same maser group showed different time variation. This phenomenon is discussed further in section 8.3,

The 1667 MHz spectrum shows a (weak) plateau of emission covering the same velocity range as the 1612 MHz emission. An absorption feature is seen at –125.9 km s^{-1}, coinciding with the edge of the 1612 MHz profile. Apparently part of the OH is seen in absorption against the galactic continuum background.

The emission spikes in the 1667 MHz spectrum are coincident in velocity with emission features in the 1612 MHz spectrum. At the time of the 1665 MHz VLA observations the 1667 MHz plateau and the –93 km s^{-1} 1612 MHz component had not yet been discovered. So, unfortunately, the band chosen to observe the 1665 MHz emission did not cover the range –85 to –110 km s^{-1}; we do not know whether the 1667 MHz plateau or the 1612 MHz maser component at –93 km s^{-1} have any 1665 MHz counterparts.

Mauersberger et al. (1988) have detected CO emission from this object. The emission peaks at –107 km s^{-1}, midway between the two main OH components. The total velocity width is 45 km s^{-1}, almost identical to the OH. While it is not clear whether the CO and the OH trace the same positions in the shell, the kinematic structure of regions where the two molecular species are found is quit similar.

4.10. OHPN 10 (IRAS 17443–2949)

The spike in the spectrum of this source resembles the blue shifted peak of other OH/IR stars. The 1612 MHz spectrum shows wide absorption near 8 km s^{-1}. The low galactic latitude ($\approx -0\overset{\circ}{.}8$) and near zero velocity suggests that the OH absorption is interstellar in nature, and not associated with OHPN 10. The positions of the IRAS source and the continuum source are consistent with each other. Preliminary results from recent VLA observations show that the OH emission coincides with the continuum source.

4.11. OHPN 11 (IRAS 17580–3111)

This is the only OHPN with more than two groups of spikes in the 1612 MHz spectrum. VLA observations are needed in order to show whether the four groups all belong to the same object. Multiple maser groups can, in general, not be produced in an envelope with a purely spherical geometry, but can be caused by strong bipolar outflows (see also Chapman, 1988). There is about 1′ difference between the continuum and IRAS source.

*4.12. OHPN 12 (*Vy 2–2*)*

Seaquist and Davis (1983) have observed this well-known source with the VLA. Their map shows a slightly elongated continuum source. The OH emission is seen projected unto the ionized region, but is displaced from the centroid of the continuum source in the direction of the major axis. This is indicative of a nonspherical morphology of the OH emitting shell.

5. Sources with uncertain classification

In this section we will discuss a number of sources which possibly also belong to the group of OHPN. For various reasons their classifications are uncertain, and the objects described here will not be included in the discussion to follow.

5.1. OH 24.8–0.0

The 2 cm VLA map shows a possible detection at the 3 mJy level. At 6 cm this could not be confirmed due to two bright HII regions located about 5′ to the south. The 1612 MHz profile published by Caswell and Haynes (1983b) shows the familiar one-sided profile. Since the possible continuum detection could not be confirmed, we have not included this source in the list of OHPN. Follow-up observations both at 2 cm and 6 cm are needed.

5.2. OH 5.89–0.39

This source is described in Zijlstra and Pottasch (1988) and Harvey and Forveille (1988). Its classification is not clear. The 1612 MHz line has rapidly decreased in strength, indicating possibly fast evolution of the central object. At the same time the main lines have not changed in intensity (Caswell and Haynes, 1983b). The central source is a strong continuum source with a bipolar morphology. A high velocity outflow is apparent from CO data presented by Harvey and Forveille. OH 5.89–0.39 is thus one of the rare sources known to exhibit both CO and strong 1612 MHz OH emission. H_2O emission is also present (Genzel and Downes, 1977). Since OH 5.89–0.39 could be a peculiar HII region instead of an OH/IR star, we have not included it in the present sample. The object clearly deserves more study to clarify its nature.

5.3. K 3–35

Engels et al. (1983) report strong 1612 MHz OH emission from this object, but also mention that the classification is not clear. Its association with a dark cloud, both in position and velocity, suggests it is a compact HII region. However, the OH line ratios are atypical of HII regions, since the 1612 MHz is much stronger than the 1667 MHz emission, and no 1665 MHz emission is observed. Caswell and Haynes (1983a) find 1612 MHz emission

from 9 out of 85 masers believed to be associoated with HII regions. In almost all these cases, however, the 1612 MHz is at most comparable in strength to the main lines. In section 9.5 we will comment on the classification of K3–35.

6. Physical characteristics of the nebulae

In Tables 2 and 3 the observational characteristics of the detected sources are listed, such as, position, radio flux density, 1612 MHz flux density and velocity, etc. NGC 6302 and Vy 2–2 are also included. The position is always that of the radio continuum source, which is accurate to within 10″. The position of the OH emission has been measured with the VLA for four sources (Vy 2–2, NGC 6302, OHPN 2 (OH 349.36–0.20; only at 1665 MHz) and OHPN 9 (OH 0.9+1.3)); the OH positions agree to within a few arcseconds with the continuum positions. For the remaining sources we have only single-dish OH measurements. The possibility of confusion for these sources is non-negligible, as shown above. VLA observations are desirable to confirm the positional association.

We have listed the velocities of the OH maser spikes. In the case of single peaks, i.e. complete absorption of the red shifted emission, this will be blueward of the actual stellar velocity. OH/IR stars generally have expansion velocities of 20 to 25 km s^{-1}. In these cases the expected stellar velocity is the quoted velocity plus 20 km s^{-1}. The actual central nebular velocity is unknown except for Vy 2–2 and NGC 6302 (−71 km s^{-1} and −56 km s^{-1} respectively). Some of the newly found objects show a high radial velocity and are probably part of the galactic bulge. These objects are therefore expected to be close to the galactic centre, at a distance of approximately 8 kpc.

We expect that most of the OHPN have significant optical depth at 6 cm, possibly even at 2 cm. At the distance of the galactic centre a spherical ionized region will have a 6 cm radio flux density:

$$S_{6\,\mathrm{cm}} = 2.5 \left(\frac{T_e}{10^{-4}\,\mathrm{K}}\right) \left(\frac{R}{10^{15}\,\mathrm{cm}}\right)^2 (1 - e^{-\tau})\,\mathrm{mJy} \qquad (1)$$

where T_e is the electron temperature in degrees Kelvin, R is the radius in cm and τ the optical depth. For $T_e = 10^4$ K and $\tau_{6\,\mathrm{cm}} = 1$, the source will be detectable at 6 cm if $R > 10^{15}$ cm. The OH emission in OH/IR stars normally occurs at radii of 10^{16}–10^{17} cm. The ionized region can be larger than 10^{15} cm without destroying the OH emitting region, and thus the object could have lower optical depth and still be detectable, even at the distance of the galactic centre. Therefore the possibility that the objects are optically thin at 6 cm cannot be ruled out. For four objects multiple frequency measurements are available; three have significant optical depth at 6 cm.

From the data we can derive a number of other quantities, listed in Table 4. The total far infrared flux is determined by summing over the IRAS bands in which the source was detected. No bolometric correction is applied. With a maximum of only four points along the far infrared spectrum, the total flux cannnot be determined very accurately. However, the values should be accurate to within a factor of two. No colour correction has been applied to the IRAS data. We assume that the objects with a high radial velocity ($|V_{\mathrm{rad}}| > 50$ km s^{-1}) are part of the galactic bulge. For those source the far infrared luminosity has been calculated. For NGC 6302 we assume a distance of 1 kpc. Its total far infrared flux density precludes a much larger distance: the luminosity would exceed the maximum luminosity allowed for PN ($\approx 2 \times 10^4$ $L_\odot$: Kippenhahn, 1981). For the other sources no luminosity is given. The far infrared luminosity probable accounts for most of the stellar luminosity.

The IRE is also listed, calculated as given in appendix A. We have used the flux density at the shortest observed wavelength. Since the nebulae might still be optically thick at this wavelength, the values given for the IRE should be considered as upper limits. This effect can be expressed in terms of the parameter a, defined as the ratio of the optically thin radio flux density (extrapolated to the observed frequency) to the measured flux density (Pottasch et al., 1987). The IRE is proportional to 1/a.

In most cases the sources are unresolved, with upper limits to the angular size of 1–3″. An order of magnitude estimate of the true size can be obtained if we assume an optical depth of

Table 3. Measured quantities of the sample of OHPN stars

#	Name	F_{6cm}	IRAS fluxes				F_{IR}	vel_{OH}		F_{1612}		Ref.
			12 μm	25 μm	60 μm	100 μm	×10^{12}					
		[mJy]	[Jy]	[Jy]	[Jy]	[Jy]	[W m^{-2}]	[km s^{-1}]		[Jy]		
1	NGC 6302	3500.	32.2	334.0	846.0	535.0	48.6	−38.	−47.	0.5	0.2	1,3
2	OH 349.36–0.20	40.	2.5	19.8	104.0		4.04		−126.		0.5	4,8,11
3	IRAS 17207–2856	8.2	< 2.5	8.0	7.6		0.61		−18.		0.4	9,11
4	PK 356+2° 1	14.3	1.3	8.7	3.7		0.72	18.	−15.	0.4	0.2	9,11
5	IRAS 17347–3139	52.0	19.2	100.0	125.0		19.7	−120.	(-20.)	0.6	(0.3)	10,11
6	IRAS 17371–2747	8.1	2.1	10.6	14.6		1.21		115.		0.8	9,11,13
7	IRAS 17375–2759	2.6	< 4.4	6.4	< 10.5		1.21		21.		1.	9,11,13
8	IRAS 17375–3000	0.8	< 5.0	19.8	< 37.2		1.02	−36.	−16.	2.8	2.6	10,13
9	OH 0.9+1.3	1.4	1.8	17.8	37.0		2.12	−124.	−93.	54.	0.5	4,11
10	IRAS 17443–2949	0.9	15.8	39.3	34.3		5.04		−15.		1.2	10,11,13
11	IRAS 17580–3111	8.9	3.3	15.4	7.8		1.43		15.		2.7	10,11
12	Vy 2 – 2	48.	15.5	94.0	42.3	10.1	8.13		−62.		5.	4,6,12

References continuum observations :

1: Payne et al. 1988; 3: Pottasch 1984; 4: Pottasch et al. 1987;
6: Seaquist and Davis 1983; 9: Pottasch et al. 1988; 10: Ratag et al. 1988; 12: Clegg and Walsh 1988
References used for the information on the OH data :

8: Caswell et al. 1983; 11: this work; 13: Olnon et al. 1981

Table 4. Derived parameters of the OHPN

#	name	IRE [a^{-1}]	L_{IR} [$10^3 L_\odot$]		θ [$''$]	size (FWHM) if $T_b = 10^3$ K	N_e [$10^3 cm^{-3}$] [$a^{\frac{1}{2}}$]	M_i [$10^{-2} M_\odot$] [$a^{\frac{1}{2}}$]	$T_\star$ [10^3 K]
1	NGC 6302	1.6			3.5◇	2.	7.3♠		> 80
2	OH 349.36-0.20	5.4♡	10.		0.4	0.3	40.	1.9	35
3	IRAS 17207-2855	7.9	1.5		1.6	0.4	2.3	7.0	33
4	PK 356+2° 1	5.4	1.8	<	1.5	0.8	9.2	3.0	35
5	IRAS 17347-3139	118.	49.3	<	1.	0.1			15
6	IRAS 17371-2747	15.9	3.0	<	1.	0.2	7.8	0.2	27
7	IRAS 17375-2759	49.6			2.3	0.1			20
8	IRAS 17375–3000	209.				0.1			16
9	OH 0.9+1.3	75. ♡	5.3	<	1.	0.1	120.	0.02	18
10	IRAS 17443-2949	611.		<	1.	0.1			13
11	IRAS 17580-3111	17.2		<	1.	0.2			24
12	Vy 2 – 2	4.3♡			0.2♣	0.3	100. ♣		35

Notes to Table 4:

♣ *Clegg and Walsh 1988*
◇ *Seaquist and Davis 1983*
♡ *Based on flux densities at higher frequencies*
♠ *Pottasch 1984*

unity at 6 cm. The brightness temperature T_b of a spherical HII region can be written as

$$T_b = T_e(1 - e^{-\tau}) = 70.7 \frac{S_{6cm}}{\theta^2} \quad (2)$$

(Kwok 1985), where S_6 cm is the radio flux density in mJy, and θ is the angular diameter in arcseconds. We assume a T_e of 10^4 K. The assumption of $\tau = 1$ at 6 cm thus yields an estimate to the angular size. When no direct size determination is available, this model size is given in Table 4 together with the measured upper limits.

The model of a spherical source with uniform density also yields the electron density and ionized mass, if the distance is known. For NGC 6302 and Vy 2–2 the density has been determined from optical observations (Pottasch, 1984 (hereafter referred to as P84); Clegg and Walsh, 1989). Table 4 lists this density for these two sources, and model densities for the sources thought to be in the galactic bulge.

7. The temperatures of the central stars

The IRE can be used to derive the stellar temperature. We make two assumptions: (1) all photons with energy above the Lyman continuum limit will ionize one and only one hydrogen atom; (2) all energy emitted by the star will eventually be absorbed by dust and reradiated in the far infrared. The second assumption implies that only a negligible fraction of the total energy comes out in forbidden lines such as oxygen and nitrogen. Especially for low excitation nebulae this assumption is reasonable. Thus we limit the application to low temperature central stars.

Starting from these assumptions, the formulae are derived in appendix B. They are given in terms of $T_\star/G_i(T_\star)$, where $G_i(T_\star)$ is a function of temperature arising from the conversion between stellar temperature and total number of ionizing quanta.

To apply this method one needs to know the *optically thin* radio flux density. Since we don't know whether our objects are optically thin at the observed wavelength, the derived IRE must be considered an upper limit, and the stellar temperature a lower limit. However, within the range of interest the temperature varies only slowly with $T_\star/G_i(T_\star)$ and thus with the IRE. If, for instance, the IRE has been overestimated by a factor of five, a temperature found to be 17,000 K should have been 23,000 K. At higher temperatures the effect becomes more severe. For Vy 2–2 the IRE would have been overestimated by a factor of five, had the 6 cm flux density been taken instead of the (known) optically thin value. Most of the uncertainty in the derived stellar temperature arises from this problem.

Taking the average between the low and high density case, and combining formulae A4 and B5 in the appendices, the relation between the IRE and $T_\star/G_i(T_\star)$ becomes:

$$T_\star/G_i(T_\star) = 1.4 \times 10^4 \times IRE \quad (3)$$

Table 4 lists the results for our sample of OHPN. In all cases the radio flux density is taken from the highest frequency point available, in order to get a better approximation to the optically thin flux density. No temperature has been determined for NGC 6302. The central star of this well-studied nebula has never been discovered, most likely because it has a very high temperature. In one case, Vy 2–2, we can immediately compare our result with stellar temperatures derived by other methods. The Zanstra

method gives about 42,000 K (Clegg and Walsh, 1989). Our result is slightly lower, but the nebula is probably already too far evolved for application of the IRE method: a significant fraction of the nebular luminosity is radiated in forbidden lines, which are ignored in our method.

The derived temperatures are much lower than normally found for central stars of PN. They seem to fill in the range between post-AGB stars, which range up to 10,000 K, and full blown PN, which start at 30,000 K. The general scenario inferred from this result will be discussed in section 8.

8. Peculiar phenomena in the OH spectra

8.1. Line locking

Fig. 1^r shows both the 1612 MHz and 1665 MHz spectrum of OH 0.9+1.3. A clear correlation is seen, with the peak of 1612 MHz corresponding to a dip in the 1665 MHz profile. The two profiles are not on the same scale. The peak in the 1665 MHz profile is almost 100 times weaker than the 1612 MHz . Fig. 2 shows the energy scheme for the relevant transitions. Both lines have the same upper level, but different ground levels. Since the 1665 MHz line needs higher excitation energies than the 1612 MHz , the 1665 MHz probably originates closer to the central star, though a large volume of overlap is possible. Field (1985) has calculated the effects when the two lines are competing for the same inverted OH population, a process called "competitive gain". Since the 1612 MHz maser is expected to be strongly saturated, the population inversion between its ground and upper state is near zero. Through the equalization of these populations the 1665 MHz transition can be pushed into absorption. Each 1665 MHz photon which gets absorbed by OH will be rapidly picked up by the 1612 MHz maser. This line locking between the two maser lines can explain the correlation in the two spectra. The process requires a redistribution mechanism between the two lowest states to keep the absorption of the 1665 MHz going. Since the direct transition is not allowed, this has to work through higher rotational or vibrational levels of the OH molecule.

8.2. Polarization

For OHPN 1, 2, 4, 9, 12 we measured the circular polarization of the 1612 MHz maser emission. The amount of polarization is about $< 10\%$, $> 80\%$, $< 30\%$, $\approx 10\%$, $< 15\%$ respectively. The 1667 MHz maser emission of OH 0.9+1.3 also is circularly polarized. The velocity resolution is insufficient to identify Zeeman pairs. The magnetic field is presumably in the order of few mGauss. Circularly polarized 1612 MHz and/or 1667 MHz emission is not usually observed in OH/IR stars, with the exception of objects (PPN's ?) like OH231.8 + 4.2, IRAS16342–3814 and IRAS15405–4945 (Morris et al., 1987; te Lintel Hekkert et al., 1988; Likkel and Morris, 1988). In these objects the masing molecules are assumed to be located in a thin shell around the star or ionized region, just as is indicated by the plateaus of maser emission in the OHPN. Whether detectable polarization can only be produced by such a thin emitting shell is not known: an alternative possibility is the existence of a velocity gradient in the shell.

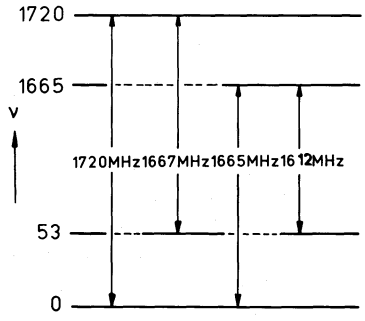

Fig. 2. The OH transition ladder

8.3. Multiple components

Many of the OHPN show OH spectra with multiple components, significantly different from thhe regular two-peaked spectrum of normal OH/IR stars. Chapman (1988) shows that these can be caused by strong bipolar outflows. Alternatively, the emitting shell may have an irregular density structure, where each individual line corresponds to a density enhancement. This could be the case for instance in NGC 6302 (Payne et al., 1988). Recently Nedoluha and Watson (1988) have proposed that a velocity gradient in the emitting shell can also cause multiple components in the maser spectrum, as well as circular polarization in the individual components. This is an attractive possibility in the case of OH0.9+1.3, where the shell is likely to be quite thick, in view of the very high intrinsic luminosity of the 1612 MHz lines. Possibly this model can also explain why some components show identical time variability, while other components covering the same velocity range vary differently. Notice that the velocity gradient would in principle need to be positive, to ensure that a gradient exists for any line of sight through the nebula. This problem may be overcome when the maser is stimulated by the radio continuum background from the inner ionized region, which would favour line of sights through the central region. Nedoluha and Watson mention that if there is no significant velocity redistribution of the OH between pumping and masing, the resulting spectrum will be broad and featureless. This could be the explanation of the plateaus of emission seen in some of the OHPN.

9. Discussion

In the following discussion we compare the observational properties of the OHPN with both ordinary OH/IR stars and PN. We exclude from the OH/IR catalogue all Mira variables and supergiants, to limit the comparison to the immediate progenitors of PN. Sources like OH231.8 + 4.2 and Vy 2–2 are also removed.

9.1. OH/IR stars versus OHPN

One way of comparing the OHPN with OH/IR stars is by the characteristics of the 1612 MHz line profiles. Most of the OH/IR stars in the OH/IR catalogue display a regular two-peak profile with steep outer and shallow inner slopes. The large majority of the remaining objects are so-called single-peaks, some of which were selected for the VLA survey (see sections 2.1.1 and 2.1.2). Most OHPN for which a good signal to noise spectrum is available show irregular profiles, with many different components. A number of the OHPN show polarization at 1612 MHz , which is non-existent (e.g.Chapman and Cohen, 1988; Reid and Moran, 1981) for the stars from the OH/IR catalogue. The high velocity outflow objects, mentioned

in section 8.2, do show these characteristics, but show emission from a much larger velocity range. On the other hand, HII regions also show irregular profiles (though mainly in the main lines, Caswell et al., 1983b), but their emission comes from a much smaller velocity range. All this suggests that the geometry of the envelopes of OHPN differs significantly from OH/IR stars; as discussed above, their envelopes could resemble high velocity objects like OH231.8 + 4.2and IRAS15405–4945.

9.2. PN versus OHPN and the importance of IRE

In order to compare the physical parameters of the OHPN and PN we plotted the distribution of the IRE for the two groups (Fig. 3). We only used the PN from Table A2. Most PN show an IRE between 1 and 3. The OHPN, on the other hand, have IRE almost ten times as high. The high IRE's imply very high visual extinction, which in turn indicates that many of the OHPN will be difficult to observe optically. Indeed most of the OHPN were first observed as infrared sources and do not have optical counterparts. The previously known PN were always first detected in the optical, either as nebulosities or as emission line objects. About 30% of the PN with IRE > 3 show 1612 MHz maser emission. Only one OHPN, NGC 6302, has IRE < 3. NGC 6302, however, is much closer than the galactic centre; at 8 kpc distance its OH emission would not have been detectable. We suggest that by the time a planetary nebula becomes optically visible, in most cases the OH maser has died either because the dust shell has diluted or the OH radicals have been dissociated. The IRE appears to be a good indicator of the age or evolutionary phase for young PN. The derived relation between the IRE and the stellar temperature points to the same conclusion.

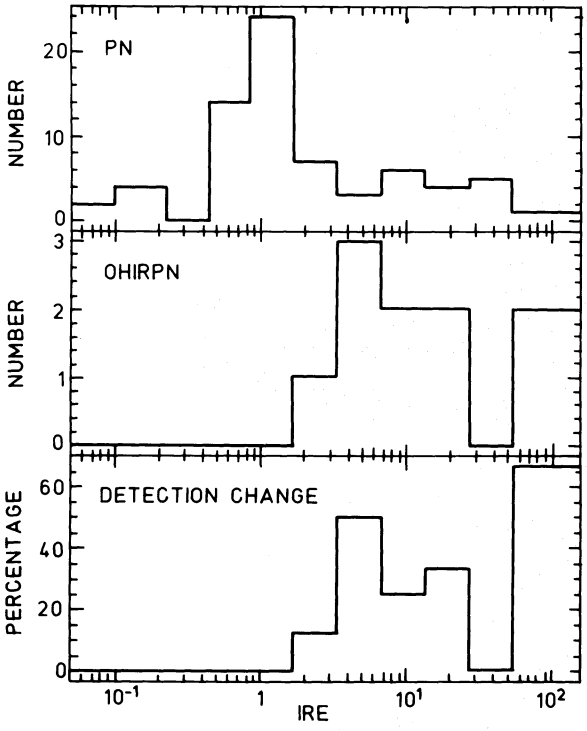

Fig. 3. Histogram of the PN, OHPN, detection of OHPN as function of IRE. The histogram borders are : .1 – .2 – .4 – .75 – 1.5 – 3. – 6. – 12. – 24. – 48. – 96. – 200.

9.3. The IRAS colour–colour diagram

In the last few years a number of authors (Bedijn, 1987 and 1988; Rowan–Robinson et al., 1986) have used the IRAS colour–colour diagram to describe the evolution from the AGB to planetary nebula. Fig. 4 shows a colour–colour diagram for the three groups of objects. From the OH/IR and PN catalogue we selected the sources with $|b| > 2.^{o}$, $|l| > 10.^{o}$; the distance between the IRAS position and object position had to be less than 0°.005 . In this way we made sure to select objects which have the most reliable flux densities and IRAS association. To make a complete picture of the evolution we also included sources like OH231.8 + 4.2 and IRAS15405–4945; the so-called high expansion velocity sources. The evolutionary status of these objects is not well known, but supposedly they are post-AGB stars which will soon evolve into PN.

The curve drawn in Fig. 5 is from Bedijn (1987) for his model 3^{c}, which describes the evolution of an oxygen rich dust shell around a star with a temperature of 2500 K, a luminosity of 10^{4} $L_{\odot}$, and with increasing mass loss.

The IRAS colours show a significantly different distribution for the different groups, but they do not clearly define an evolutionary sequence from the OH/IR stars to OHPN to the PN. The OH/IR stars are situated in a well defined area of the diagram, although there are a few very cool objects among this group. The spread in colours among PN and OHPN on the other hand is very large. Four PN are located in the part of the diagram occupied predominantly by Mira variables. Two of them (pk258-3.1 and pk312-2.1) are misclassified symbiotic stars, according to Acker et al. (1987). The other two (pk274+2.1 and pk346+8.1) are poorly studied emission line objects; we suggest that they also are symbiotic stars. The large spread in colour for the remaining PN, however, is clearly real. Geometrical effects (e.g. differences in inclination of PN with a bipolar morphology),

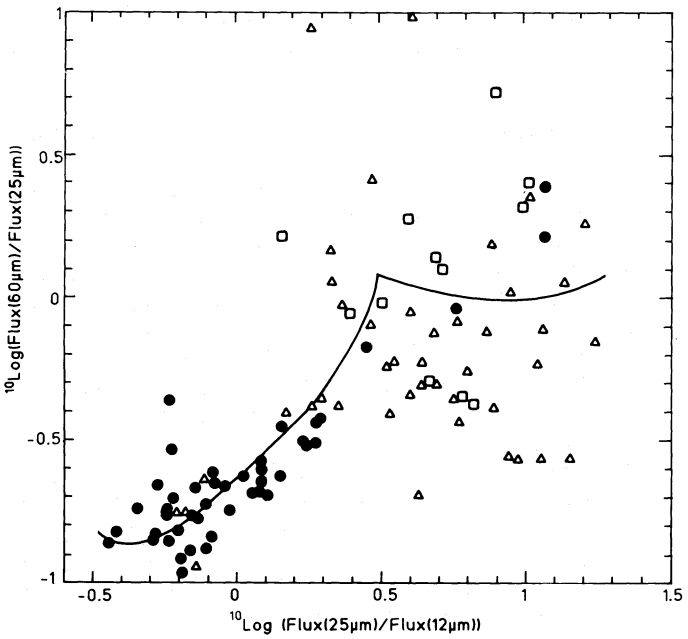

Fig. 4 . The IRAS colour–colour diagram. We plotted three groups of objects:

- OH/IR stars ($|b| \geq 2.^{o}0$, $|l| \geq 10.^{o}0$) from the OH/IR star catalogue;
- ■ OHPN;
- △ PN ($|b| \geq 2.^{o}0$, $|l| \geq 10.^{o}0$) from table A2.

differences in density and dust content of the PN envelopes, and different radiation fields will all contribute to a large scattering in the diagram. Also, for evolved PN a significant part of the infrared flux arises from emission lines instead of dust emission. In the case of NGC 7293, Leene and Pottasch (1987) have shown that especially the 12 and 25μm flux densities are effected by emission lines.

9.4. Evolutionary status and classification of PPN

The OHPN probably form an evolutionary phase immediately before the formation of a full-blown PN. The evolutionary status can be defined on the basis of the temperature of the central star, $T_\star$. This is not often used in the literature (e.g. van der Veen, 1988), since obviously it is difficult to determine the temperature of a totally obscured object. Still, $T_\star$ is the most relevant physical parameter to describe the post-AGB evolution. A second parameter, even more difficult to determine, is the evolutionary time scale. This parameter describes whether a star will evolve fast enough to ionize the surrounding nebula before it merges with the interstellar medium. The time scales are critically dependent on the core mass of the star (Iben and Renzini, 1983). A high core mass, for example, will cause the star to evolve rapidly after leaving the AGB, thus ionization of the circumstellar envelope will quite certainly take place. The OHPN, which still have a dense circumstellar envelope dust shell in combination with an already hot star, are most likely part of that group.

We propose the following classification scheme for this evolutionary phase:

1. **AGB stars**. During this phase the circumstellar shell is formed by heavy mass loss. OH/IR stars, Miras, Carbon stars, and probably the so-called S stars all contribute to the stellar population at the AGB. This phase ends when the high mass loss terminates, though a residual mass loss can still significantly influence the later stages of the evolution. $T_\star$ is in the range between 2×10^3–4×10^3 K.
2. **Post-AGB**. After the termination of the high mass loss, $T_\star$ starts to increase. Recently many objects have been found which show $T_\star$ in the range of 5×10^3–1.5×10^4 K. They form a diverse group, presumably because of a large range in core mass. The group includes the non-variable OH/IR stars (Sun and Kwok, 1987), the F to K supergiants found in the galactic halo (Parthasarathy and Pottasch, 1986), but also objects found by IRAS (Likkel et al., 1987; Volk and Kwok, 1988) and possibly the RV Tauri stars (Jura, 1986). The 1612 MHz OH sources with very high expansion velocities (Likkel and Morris, 1988; te Lintel Hekkert et al., 1988) are probably also at this stage of evolution, though their status is not well known.
3. **Early PN**. In this category are stars with temperatures between 1.5×10^4 and 2.5×10^4 K. The phase starts when the star becomes sufficiently hot to cause detectable ionization of the envelope. Most of the OHPN are found here. In general this group consists of the PN with high IRE, of which the OHPN are a subset. The high temperature limit is chosen where optical observations start to find the emission lines. This value, however, is not very well defined and might vary between different objects.
4. **PN**. At temperatures above about 3×10^4 K the object has become a full-blown planetary nebula. Some objects in this stage still show evidence of a neutral envelope, but the inner envelope is strongly ionized and the internal extinction no longer obscures the source. PN which show clear OH or CO emission, like NGC 7027, NGC 6302 and Vy 2–2, probably have the most massive central stars. They have evolved rapidly, and thus the circumstellar shell is still quite dense. Exceptions to this are NGC 2346 and NGC 7293, which show CO emission but have a much lower density. Most PN, however, do not show such molecular emission.

In this scheme the OHPN are mainly found in group 3, but some (massive?) objects with a further evolved central star also show the same characteristics. Thus the OHPN do not form a completely uniform group.

9.5. Expected numbers and life time of OHPN

In the galactic bulge the Carbon stars acount for about 20% of the total stellar population at the AGB (Knapp, 1988); the fraction varies with position both in the galaxy and in the Magellanic clouds. During a dredge-up phase, when convection brings nuclear processed material from the core to the surface, a star can change from oxygen rich to carbon rich (Willems and de Jong, 1988). Supposedly, a change the other way is not possible, and thus the fraction of carbon stars increases during the AGB (Chan and Kwok, 1988). The percentage of carbon rich PN is about 50% (Zuckerman and Aller, 1987). Thus the percentage of oxygen rich sources in the bulge in the transition phase between the AGB and PN will be between 50% and 80%. The actual detection rate of OH emission will be lower, since the maser will be adversely effected by the dilution and ionization of the envelope. We do not expect to detect any OH maser emission from carbon rich nebulae since almost all oxygen is locked in CO.

An estimate of the total number and lifetime of the OHPN can be obtained as follows. We estimate the number of OH/IR sources in the galactic bulge which were detected by IRAS, $N_{OH/IR} = 1500$ (Habing et al., 1989). The average lifetime of the OH/IR star stage, $t_{OH/IR}$, is probably about 10^3–5×10^3 years, as indicated by the angular size and expansion velocity of known OH/IR stars. About 20% of the IRAS sources in the bulge with PN colours are PN with with an IRE exceeding 3 (preliminary result from Ratag et al., 1989). The OH detection rate for these sources is again about 30%. With 3000 IRAS sources in the galactic bulge with PN colours we estimate the total number of OHPN as approximately $N_{OHPN} = 200$. The lifetime of the OHPN phase, t_{OHPN}, can be written as:

$$t_{OHPN} = \frac{N_{OHPN}}{N_{OH/IR}} \times t_{OH/IR} \times \frac{1}{f} \qquad (4)$$

where f is the fraction of the OH/IR stars which will pass through this phase. We obtain $f \times t_{OHPN} \approx 100$–$500\,yr$. These values are not unreasonable. Sun and Kwok (1987) and Burrajabel et al. (1988) derive a transition time from the AGB to PN of about 10^3 yr, which is thus an upper limit to t_{OHPN}. Our derived value would indicate that many of the OH/IR stars will become OHPN sources; however, better statistics are needed to really quantify the percentage. The life time of the OHPN phase cannot be much shorter than 100 yr, or the changes in the spectrum would be easibly observable on a time scale of a few years.

The resulting birth rate of OHPN is approximately 1 per year. Pottasch (P84, p121) estimates that the birth rate of PN is 1–2 per year, which is in reasonable agreement. It appears that a

significant fraction of the PN will have passed through the phase of OHPN.

9.6. The classification of OH sources on basis of their line strength ratios

The classification scheme for OH maser emission is defined by Turner (1970, 1973). In this scheme strong 1612 MHz emission in combination with weak or absent main line emission is taken as evidence for evolved objects (e.g. OH/IR stars); the source would be classified as Type IIb maser object. Type I or main line masers are assumed to be associated with either Miras or the compact cores of HII regions (Reid and Moran, 1981). This classification scheme does not hold for objects like OH231.8 + 4.2, IRAS15405–4945, and the OHPN, which are closely associated with the OH/IR stars, but often show line ratios more characteristic for Miras or even HII regions. In quite a few cases the main lines are comparable to or even stronger than the 1612 MHz line. The physical reasons could be: (1) the shell is probably quite thin, resulting in a short pathlength of the OH maser; (2) the harder radiation field, caused by the hot central star, will cause different excitation conditions for the OH radicals; (3) in addition to the infrared pump, other pumps for the maser transitions might be at work. An additional difference is that the maser is amplifying the radio continuum background instead of the spontaneous emission of the OH radical. In these circumstances it is not clear which OH maser line will dominate the radiation and, thus, how the source will be classified. The effect of a shorter path length has been calculated by Field (1985): he finds that the main lines, especially the 1667 MHz line, become stronger relative to the 1612 MHz . Note that the effect of a velocity gradient in the shell will be similar, since the pathlength at each particular velocity will be shortened.

In the case of K 3–35, which on the basis of velocity and positional information would be classified as an HII region, the presence of a strong 1612 MHz maser is puzzling, and raises the question whether HII regions can sometimes resemble OH/IR stars.

The scheme should be carefully applied and whenever possible supplemented by other evidence such as velocities. This applies to our sample of OHPN as well: objects closely confined to the galactic plane, and with velocities allowed by galactic rotation, could be misclassified. For instance, OHPN 2 satisfies these two criteria. It also has the lowest colour temperature of the sample; thus, further information is needed to ensure it is not a compact HII region. Mauersberger et al. (1988) have failed to detect CO emission from the vicinity of OHPN 2. This argues against the presence of a large molecular cloud, and therefore favours a classification as evolved object.

10. Conclusions

Maser emission at 1612 MHz is found in a number of young PN. The objects are thought to be in a short lived transition phase between OH/IR stars and PN. All of these so-called OHPN have high infrared excess, and thus low stellar temperatures. The derived temperatures imply that they are still in transition towards planetary nebula. We estimate that the total number of OHPN in the bulge is about 200, and their life time is of the order of 100 yr. The resulting birth rates imply that many PN will have passed through this phase.

The OHPN have OH spectra which strongly differ from those of OH/IR stars. The profiles are irregular and sometimes show significant polarization. One object, OHPN 9, is one of the intrinsically strongest 1612 MHz emitters in the galaxy. Its peak flux density has increased by a factor of 2 in 15 years, and evidence has been found for large variations at much shorter time scales.

The traditional classification scheme for OH maser emission does not always apply to these post-AGB objects; especially for objects in the galactic plane one should be careful with classifying them purely on the basis of OH line ratios.

The sample of OHPN constitutes the best defined group in this evolutionary phase as yet. In some cases the problem of confusion still needs to be addressed: accurate positional information on the OH emission from the OHPN will hopefully be obtained in the near future.

Acknowledgements. Te Lintel Hekkert and Zijlstra received grants in support of this research project from the Netherlands Foundation for the advancement of pure research (NWO), through its working group ASTRON. The NRAO is operated by the Associated Universities Inc., under contract with the National Science Foundation. We thank Orla Aaquist, A. LeSqueren and Lauren Likkel for their careful reading of the manuscript, and the many improvements they suggested. Ray Norris, Ray Haynes, Huub Röttgering and Sabine du Croo de Jongh are gratefully acknowledged for their support during the observations in Australia. We especially thank Dr. C. Bignell for his help with the VLA observing and data reduction. The staff at the VLA is remembered for their unwavering help to "those students".

Appendix A. The InfraRed Excess

The Infrared Excess (IRE), defined by Gatle et al. (1978), is defined as the ratio of the observed total far infrared flux over the far infrared flux due to absorption by dust of Ly_α photons:

$$IRE = \frac{F_{ir}^{obs}}{F_{ir}^{exp}} \qquad (A1)$$

In calculating F_{ir}^{exp}, each stellar photon shortward of 912 Å is assumed to ionize a hydrogen atom. The subsequent recombination will eventually lead to a photon from the Lymann series. However, since the optical depth in the Lymann lines is very high, this photon will soon be reabsorbed. After a number of absorption and re-emission events, this will lead to a photon from the Balmer series, plus a Ly_α photon. The Balmer photon will escape from the nebula, since the optical depth in the Balmer lines is low. This effect is used in the Zanstra method for determining stellar temperatures (Zanstra, 1931).

After many scattering events, the Ly_α photon will most likely be absorbed by dust. If all the energy seen in the far infrared can be explained by this process, the $IRE = 1$. If the far infrared flux is larger, the $IRE > 1$. Since each Ly_α photon is accompanied by a photon from the Balmer series, we can predict the amount of far infrared flux from one of the Balmer lines, like H_β. Let α_B be the total recombination coefficient of all Balmer transitions, and α_{H_β} that of the H_β transition alone. It follows:

$$F_{Ly_\alpha} = \frac{\nu_{Ly_\alpha}}{\nu_{H_\beta}} \frac{\alpha_B}{\alpha_{H_\beta}} F_{H_\beta} \qquad (A2)$$

If the density is low ($n_e < 10^4\,\mathrm{cm}^{-3}$), a correction has to be applied for recombination through the 2^2S level, which does not produce Ly_α. At higher densities collisions prevent such recombination.

The optically thin radio flux density S_ν can be used to calculate the expected H_β flux density (P84, p93). We have put the electron temperature $T_e = 10^4$ K, and the helium abundance factor $Y = 1.1$ (equivalent to assuming all helium to be in the singly ionized state). Using the radio flux density at 5 GHz, we find:

$$F_{ir}^{exp} = \begin{cases} 0.75\,S_5 & (n_e < 10^4\,\mathrm{cm}^{-3}) \\ 1.11\,S_5 & (n_e > 10^4\,\mathrm{cm}^{-3}) \end{cases} \qquad (A3)$$

where F_{ir}^{exp} is in units of $10^{-14}\mathrm{Wm}^{-2}$ and S_5 in mJy. Finally:

$$IRE = \begin{cases} 1.33\,\frac{F_{ir}^{obs}}{S_5} & (n_e < 10^4\,\mathrm{cm}^{-3}) \\ 0.91\,\frac{F_{ir}^{obs}}{S_5} & (n_e > 10^4\,\mathrm{cm}^{-3}) \end{cases} \qquad (A4)$$

In applying this formula, we have taken the average of the low — and high density case. For high density objects we will have overestimated the IRE by 20%.

A completely different definition of the infrared excess is also used in the literature, namely dividing F_{ir}^{obs} by the expected stellar continuum (e.g. Pottasch and Parthasarathy, 1986). These two definitions should not be confused.

Appendix B. Derivation of the temperatures of the central stars

This method to determine the temperature of the central star of a planetary nebula has not yet been discussed in the scientific literature. We therefore include a description of the technique, which is a variation on the Zanstra method (Zanstra, 1931). This way of determining the stellar temperature applies to those central stars where most of the stellar emission is absorbed by dust in the nebula and reemitted in the far infrared. It does not require direct observations of the star, and the determined temperature is independent of any assumption concerning the distance of the star. If the distance is known, however, the stellar radius can be determined as well, similar to the Zanstra method.

The physical reason for the determination is simple. If a model of the flux emission is known, for example a blackbody distribution, and both the total flux and the number of ionizing photons are known, there is only one temperature that will reproduce the observed ratio of the two quantities. The total flux is approximated by the total far infrared flux (F_{ir}), while the number of ionizing photons is determined from the observed radio flux density. This assumes that each photon with sufficient energy to ionize a hydrogen atom will indeed do this, and is not absorbed by, for example, the dust. The method therefore works best for the low temperature stars of very young PN, where both assumptions are approximately true.

To make this quantitative the star will be assumed to radiate as a blackbody, although a similar analysis can be made for any known model atmosphere. Many of the equations given are discussed more fully in P84. The observed H_β flux density, F_{H_β}, can be written as

$$4\pi d^2 F_{H_\beta} = h\nu_{H_\beta} \int n_e n_p \alpha(H_\beta) dV = h\nu_{H_\beta} \frac{\alpha(H_\beta)}{\alpha_B} \qquad (B1)$$

where d is the distance to the nebula, $\alpha(H_\beta)$ is the recombination coefficient for producing the H_β line and α_B is the effective total recombination coefficient to levels 2 and higher (equations VII-10,11 and Table VII-5, P84). The integral is over the total emitting volume. Q_i is the number of stellar quanta which can ionize hydrogen (equation VII-9, P84)

$$Q_i = \frac{15 G_i(T_\star) L_\star}{\pi^4 k T_\star} \qquad (B2)$$

where $T_\star$ is the stellar temperature, $L_\star$ the luminosity and $G_i(T_\star)$ a function of temperature (eqn. VII-8 and Table VII-4, P84). Combining these equations we obtain:

$$\frac{T_\star}{G_i(T_\star)} = \frac{h\nu_{H_\beta}}{k\pi^4} \frac{\alpha(H_\beta)}{\alpha_B} \frac{15 L_\star}{4\pi d^2 F_{H_\beta}} \qquad (B3)$$

If we assume an electron temperature in the nebula of 10^4 K and a He^+/H ratio of 0.1, the H_β flux can be written as

$$F_{H_\beta} = \frac{S_\nu}{3.10 \times 10^{12}} \qquad (B4)$$

where S_ν is the 6 cm continuum flux density in mJy. The units of F_{H_β} are erg cm^{-2} s^{-1}. Then

$$\frac{T_\star}{G_i(T_\star)} = \frac{8.43 \times 10^2}{S_\nu} \frac{L_\star}{L_\odot} \left(\frac{8\ \mathrm{kpc}}{d}\right)^2 = 1.65 \times 10^{18} \frac{F_{ir}}{S_\nu} \qquad (B5)$$

where F_{ir} is the total infrared flux in units of Wm^{-2}. Thus $T_\star/G_i(T_\star)$ can be determined from the observational parameters. Since G_i is a known function of temperature $T_\star$ can now be determined. For a blackbody the function is shown in Fig. B1 and listed in Table B1. Notice that the function is multivalued; we limit ourselves to values of $T_\star/G_i(T_\star) > 10^5$ where we are certain that the low temperature result is the correct one. The physical reason for the different possible solutions lies in the assumption that each stellar photon can ionize only one atom: at higher temperatures the total number of ionizing photons starts to decrease again.

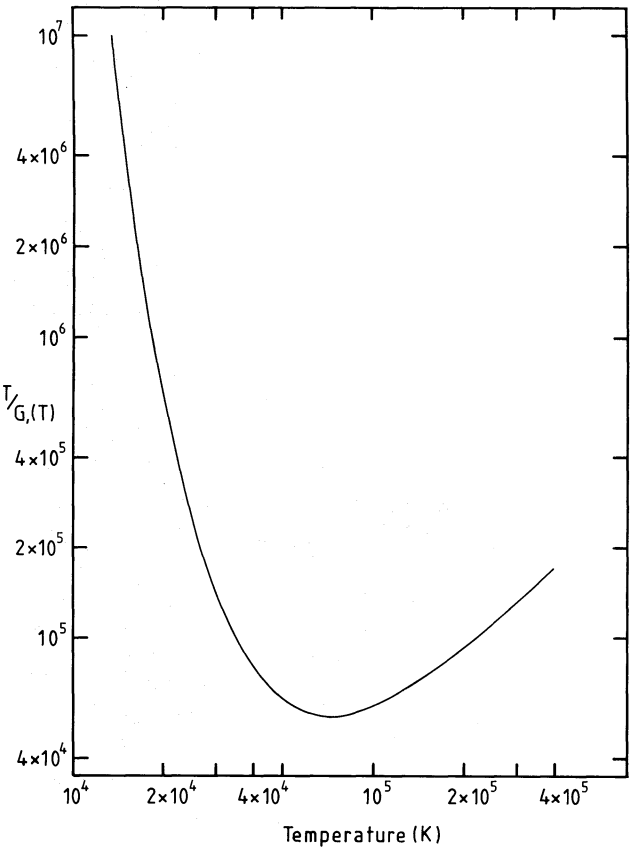

Fig. B1. Relation between stellar temperature and IRE

Table B1. Relation between stellar temperature and IRE

$T_\star$ [K]	$T_\star/G_i(T_\star)$	IRE
13,500 K	9.94×10^6	710.0
15,000 K	4.16×10^6	297.0
16,500 K	2.09×10^6	149.0
18,000 K	1.20×10^6	85.7
20,000 K	6.70×10^5	47.9
25,000 K	2.50×10^5	17.9
30,000 K	1.44×10^5	10.2
40,000 K	8.07×10^4	5.8

If the distance is known the total luminosity of the star can be determined from

$$4\pi d^2 F_{ir} = L_\star \qquad (B6)$$

or

$$\left(\frac{8}{d}\right)^2 \frac{L_\star}{L_\odot} = 1.96 \times 10^{15} F_{ir} \qquad (B7)$$

Since the stellar temperature has been determined, the stellar radius can be found from

$$\left(\frac{R}{L_\odot}\right)^2 = \frac{L_\star}{L_\odot}\left(\frac{T_\odot}{T_\star}\right)^4 \qquad (B8)$$

Appendix C Tables

Table C1. VLA continuum observations of OH/IR stars

Name or l	b	α	δ	flux density upper limit at 2 cm [mJy]	Ref.
355.581	21.114	$16^h16^m39^s$	-19°43′26″	1.2	11
338.445	−0.383	16 39 08	-46 34 51	2.3	11
343.003	0.905	16 50 14	-42 16 41	1.8	11
353.366	7.728	16 55 57	-29 57 11	1.4	11
345.957	0.611	17 01 15	-40 09 07	1.7	11
353.433	6.081	17 02 12	-30 54 11	1.3	11
351.839	1.923	17 13 38	-34 39 00	1.9	11
355.068	3.874	17 14 59	-30 53 31	1.3	11
OH 349.36−0.2		17 15 04	-37 54 53	detected	2
357.495	4.891	17 17 33	-28 19 37	1.1	11
358.687	5.161	17 19 36	-27 11 48	1.1	11
351.118	−0.353	17 20 45	-36 33 00	1.6	11
OH 0.1+5.1		17 23 23	-26 02 24	1.4	3,4,5
1.461	5.606	17 24 50	-24 39 32	1.3	11
358.367	2.806	17 27 38	-28 46 44	1.3	11
OH 354.88−0.54		17 31 33	-33 31 34	1.4	1
OH 359.75+1.25		17 31 45	-27 43 16	1.5	3
354.487	−1.462	17 34 27	-34 21 39	1.6	11
358.955	1.296	17 34 53	-29 06 39	1.6	11
OH 356.50−0.55		17 35 58 .1	-32 10 21	1.4	1
355.640	−1.741	17 38 34	-33 32 14	1.5	11
0.936	1.416	17 39 14 .0	-27 22 26	1.3	11
OH 0.9+1.3		17 39 24	-27 27 05	detected	4,5
OH 1.21+1.26		17 40 29	-27 13 28	1.6	3
1.369	1.001	17 41 51	-27 13 33	1.7	11
OH 1.09+0.38		17 43 34 .5	-27 48 49	1.9	3
4.007	0.917	17 48 17 .5	-25 01 07	1.5	11
OH 5.0+1.5		17 48 24 .4	-23 50 55	1.4	3,4,5
8.904	3.715	17 48 47	-19 22 59	1.7	11
OH 10.4+4.6		17 48 54	-17 41 41	1.9	6
357.213	−3.697	17 50 29	-33 12 50	1.5	11
OH 13.1+5.1		17 52 53 .2	-15 03 17	1.7	6,7
14.809	5.927	17 53 14	-13 11 20	1.6	11
OH 2.19−1.66		17 54 05	-27 53 57	1.8	1,3
359.621	−3.293	17 54 34 .6	-30 56 10	1.5	11
OH 7.95+1.45		17 55 04	-21 20 54	1.5	1,3,4,5
358.435	−4.498	17 56 42	-32 33 50	1.3	11

continued

Name or l	b	α	δ	flux density upper limit at 2 cm [mJy]	Ref.
OH 5.88–0.39		17 57 26 .7	-24 03 56	detected	1,3,5
10.327	1.445	18 00 08	-19 18 00	1.3	11
9.104	0.296	18 01 48	-20 55 54	1.3	11
3.684	–3.345	18 04 00	-27 26 20	1.7	11
OH 12.8+0.9		18 07 10 .6	-17 27 34	1.4	8
OH 11.56+0.09		18 07 42	-18 53 40	1.8	1,5,6
OH 15.4+1.9		18 08 42 .9	-14 40 43	1.3	8
OH 20.8+3.1		18 15 14 .0	-09 19 55	1.1	7
OH 16.12–0.29		18 18 15 .2	-15 04 47	1.3	1,6
OH 18.38+0.16		18 21 01 .9	-12 52 13	1.4	5,6,7
OH 17.0–1.2		18 23 24 .6	-14 44 10	1.4	6,7
OH 19.2–1.0		18 26 40 .1	-12 39 57	1.4	5,9
OH 20.43–0.34		18 26 48 .5	-11 17 56	1.4	1,5
17.543	–1.926	18 27 00	-14 35 35	1.5	11
OH 17.7–2.0		18 27 39 .5	-14 31 00	1.4	8
15.663	–3.708	18 29 56	-17 05 02	1.5	11
4.108	–9.770	18 30 51	-30 03 18	1.5	11
OH 23.75+0.21		18 31 06 .4	-08 06 28	2.1	1,5,6
OH 24.8–0.1		18 34 03 .6	-07 20 52	detected ?	5
OH 25.5–0.3		18 36 09 .0	-06 47 32	2.3	6
10.817	–13.320	18 58 01	-25 36 29	1.4	11
OH 37.1–0.9		18 59 36 .2	03 15 53	1.6	5
43.502	1.212	19 04 09	09 52 35	1.3	10
47.761	3.123	19 05 17	14 31 59	2.6	10
OH 42.60+0.07		19 06 34 .5	08 32 56	1.3	1,5
60.200	2.040	19 34 27	24 57 28	1.7	10
60.014	–2.198	19 50 03	22 39 47	1.7	10
64.359	–5.621	20 12 47	24 30 05	1.8	10
70.477	–17.565	21 10 02	22 05 35	1.7	10

Notes to Table A1:

1: Fix and Mutel, 1984; 2: Caswell et al., 1981; 3: Baud et al., 1979a;
4: Kerr and Bowers, 1974; 5: Winnberg et al., 1981; 6: Bowers and De Jong, 1983;
7: Baud et al., 1979b; 8: Bowers, 1978; 10: Eder et al., 1988
11: te Lintel Hekkert et al., 1988b

Table C2. OH observations of Planetary Nebulae: non detections

Name	VEL_{PN} [km s^{-1}]	6 cm flux density [mJy]	Ref. PN	IRAS name	F_{IR}^{TOT} $\times 10^{12}$ [W m^{-2}]	IRE	velocity range [km s^{-1}]		3 σ [Jy]	Ref. OH
PK 120+ 9° 1	–13.00	460.00	1	00102+7214	7.6	1.76				5
PK 118–74° 1	–46.00	247.00	1	00445–1207	0.13	0.12				5
PK 161–14° 1	–21.00	45.00	1	03531+3343	0.37	0.88				5
PK 165–15° 1	48.00	288.00	1	04061+3038	0.52	0.19				5
PK 146+ 7° 1		17.50	2	04215+6000	1.2	7.20	–316.	279.	0.09	1
PK 166– 6° 1		18.00	2	04395+3601	150.	121.82				5
PK 190–17° 1	–38.00	20.00	2	05028+1038	0.11	0.60				5
PK 215–24° 1	43.00	1550.00	1	05251–1244	18.	1.26				5
PK 176+ 0° 1			3	05345+3157	17.		–316.	279.	0.12	1
PK 184– 2° 1	26.00	69.00	2	05437+2420	0.86	1.32				5
PK 221–12° 1	35.00	178.00	2	06194–1257	0.88	0.53				5

Name	VEL_{PN} [km s^{-1}]	6 cm flux density [mJy]	Ref. PN	IRAS name	F_{IR}^{TOT} $\times 10^{-12}$ [W m^{-2}]	IRE	velocity range [km s^{-1}]		3 σ [Jy]	Ref. OH
PK 194+ 2° 1	33.00	109.00	2	06230+1749	1.0	1.02				5
PK 211- 3° 1		86.00	2	06331-0003	1.1	1.39				5
PK 212+ 4° 1	129.00	22.00	2	07026+0251	0.17	0.85				5
PK 215+ 3° 1	10.00	86.00	1	07068-0043	0.44	0.55				5
PK 232- 4° 1	-5.00		3	07090-1946	5.9		-185.	187.	0.30	2
PK 235- 3° 1			3	07172-2138	1.1		-185.	187.	0.60	2
PK 189+19° 1	11.00	87.00	1	07224+2935	0.68	0.83				5
PK 197+17° 1	64.00	251.00	1	07262+2100	1.3	0.53				5
PK 234+ 2° 1	45.00	371.00	2	07396-1805	3.3	0.95				5
PK 252- 4° 1			3	07511-3636	0.63		-186.	187.	0.60	2
PK 258- 3° 1			3	08124-4133	32.		-186.	187.	0.60	2
PK 268+ 2° 1			3	09143-4516	2.3		-185.	187.	0.30	2
PK 275- 3° 1			3	09164-5426	0.74		-185.	187.	0.30	2
PK 274+ 2° 1			3	09394-4909	2.0		-185.	187.	0.27	2
PK 261+32° 1	-8.00	860.00	1	10223-1823	4.1	0.51				5
PK 291- 4° 1	2.00		3	10583-6458	3.3		-185.	187.	0.60	2
PK 148+57° 1	11.00	101.00	2	11119+5517	0.11	0.12				5
PK 294- 4° 1			3	11295-6541	0.53		-185.	187.	0.30	2
PK 296- 6° 1			3	11369-6835	0.46		-185.	187.	0.30	2
PK 294+43° 1	8.00	205.00	1	12219-1830	0.84	0.44				5
PK 123+34° 1	-31.00	95.00	1	12317+8250	0.73	0.82				5
PK 305+ 1° 1			3	13064-6103	11.		-285.	187.	0.60	2
PK 318+41° 1	40.00	66.00	2	13379-1938	0.083	0.13				5
PK 312- 2° 1			3	14103-6311	6.2		-185.	187.	0.30	2
PK 321+ 3° 1			3	14562-5406	34.		-285.	87.	0.60	2
PK 342+27° 1	53.00	22.00	2	15193-2326	0.19	0.91				5
PK 325+ 4° 1			3	15214-5109	0.37		-186.	187.	0.14	2
PK 330+ 4° 1			3	15476-4836	5.2		-185.	187.	0.60	2
PK 64+48° 1	20.00	10.00	1	16027+4049	0.10	1.09				5
PK 331- 1° 1	-33.00		3	16133-5151	38.		-285.	87.	0.60	2
PK 346+ 8° 1			3	16307-3459	1.3		-316.	279.	0.08	1
PK 331- 5° 1	-4.00		3	16336-5536	0.83		-185.	187.	0.30	2
PK 352+11° 2			3	16416-2758	4.0		-316.	279.	0.11	1
PK 43+37° 1	-18.00	260.00	1	16423+2353	2.6	1.09				5
PK 345+ 4° 1			3	16433-3831	0.50		-261.	112.	0.29	2
PK 347+ 5° 1	-101.00	61.50	2	16456-3542	2.5	4.27	-285.	87.	0.60	2
PK 325-12° 1			3	16498-6409	0.55		-285.	111.	0.16	2
PK 0+12° 1	-21.00	118.00	2	16585-2145	1.1	1.00				5
PK 350+ 4° 1	-12.00	61.00	2	17013-3355	1.3	2.27	-316.	279.	0.06	1
PK 10+18° 2	105.00	42.00	2	17028-1004	16.	41.63	-191.	191.	0.31	1
		4.37	4	17079-3926	1.3	31.62				1
PK 358+ 5° 1	13.00	280.00	2	17180-2708	2.4	0.91	-316.	279.	0.17	1
PK 6+ 8° 1	102.00		3	17260-1913	0.42		-111.	287.	0.17	2
PK 2+ 5° 1	-90.00	1950.00	1	17262-2343	8.0	0.44				5
PK 358+ 3.8	211.00	9.80	2	17280-2812	0.55	6.04	-285.	87.	0.60	2
PK 358+ 1° 1	-282.00		3	17320-2901	0.40		-285.	261.	0.49	2
PK 358+ 1° 3			3	17321-2943	1.4		-285.	287.	0.14	2
		2.30	5	17375-2742	0.54	24.99	-186.	226.	0.15	2
		4.50	5	17401-3052	1.1	25.47				
		2.40	5	17413-2719	0.49	21.74	-316.	279.	0.29	1
PK 358- 0° 2	5.00	398.00	2	17427-3010	13.	3.39				5
PK 355- 2° 3	-182.00		3	17427-3402	0.43		-285.	261.	0.12	2
		1.10	5	17440-2321	0.12	11.68				
PK 355- 3° 1	-114.00	12.00	2	17445-3405	1.4	12.48	-316.	279.	0.13	1
		15.30	5	17448-2131	0.98	6.85				
PK 8+ 3° 1	29.00		3	17462-1959	2.5		-316.	279.	0.13	1
		5.46	4	17466-3031	0.71	13.93	-316.	279.	0.14	2
		2.20	5	17474-2738	1.2	60.39				

Name	VEL_{PN} [km s^{-1}]	6 cm flux density [mJy]	Ref. PN	IRAS name	F_{IR}^{TOT} $\times 10^{-12}$ [W m^{-2}]	IRE	velocity range [km s^{-1}]		3 σ [Jy]	Ref. OH
PK 7+ 1° 1	24.00	243.00	2	17521–2144	2.2	0.97	-316.	279.	0.17	1
		7.40	5	17550–2741	0.52	7.43				
PK 1– 2° 2			3	17552–2920	0.41		-261.	261.	0.59	2
PK 96+29° 1	-51.00	850.00	1	17584+6638A	11.	1.37				5
PK 2– 2° 4	226.00		3	17585–2825	0.79		-180.	180.	0.60	2
PK 356– 5° 2	182.00	2.70	2	17587–3427	0.75	29.52	-316.	279.	0.17	1
PK 358– 5° 2	5.00		2	18001–3242	0.30		-285.	87.	0.60	2
PK 34+11° 1	10.00	1260.00	2	18096+0650	15.	1.24				5
PK 1– 6° 2	-7.00		3	18129–3053	7.5		-85.	287.	0.60	2
PK 2– 6° 2	9.00	8.80	2	18131–3008	0.65	7.84	-110.	262.	0.60	2
PK 337–18° 1			3	18138–5712	2.1		-185.	187.	0.60	2
PK 38+12° 1	23.00	65.00	2	18152+1007	1.2	1.89				5
PK 9– 5° 1	26.00	275.00	2	18226–2313	3.3	1.26	-316.	279.	0.34	1
PK 27+ 4° 1	106.00		3	18240–0244	5.4		-316.	279.	0.10	1
PK 11– 6° 1			3	18335–2151	0.66		-316.	279.	0.12	1
PK 11– 9° 1		66.00	2	18435–2330	1.2	1.94	-180.	180.	0.60	2
PK 51+ 9° 1	36.00	108.00	2	18476+2047	1.1	1.07				5
PK 32– 3° 1		10.70	2	18579–0216	1.6	15.53	-95.	196.	0.28	1
PK 33– 2° 1	-58.00	153.00	2	19000–0031	0.90	0.63				5
PK 27– 9° 1	165.00	66.00	2	19137–0908	0.28	0.45				5
PK 46– 4° 1	30.00	89.00	2	19289+0956	0.99	1.19				5
PK 61+ 3° 1			3	19309+2646	1.4		-145.	167.	0.31	1
PK 64+ 5° 1	-13.00	630.00	2	19327+3024	29.	4.91				5
PK 57– 1° 1			3	19431+2112	1.2		-316.	279.	0.06	1
PK 83+12° 1	11.00	385.00	1	19434+5024	4.1	1.13				5
PK 68+ 3° 1		20.00	2	19499+3251	0.11	0.59				5
PK 60– 3° 1	-28.00	1325.00	1	19574+2234	1.2	0.10				5
PK 67– 0° 1			3	20011+3024	2.2		-316.	279.	0.15	1
PK 63– 3° 1			3	20028+2518	0.12		-204.	204.	0.02	3
PK 68– 2° 1			3	20119+2924	3.7		-316.	279.	0.16	1
PK 58–10° 1	-47.00	71.00	2	20178+1634	2.0	3.00				5
PK 71– 2° 1	-146.00	124.00	2	20190+3219	2.2	1.92				5
PK 93+ 5° 2	-60.00	217.00	2	20590+5420	2.9	1.44	-316.	279.	0.18	1
PK 37–34° 1	-36.00	750.00	1	21014–1133	6.6	0.93				5
PK 89+ 0° 1	-25.00	260.00	1	21046+4739	2.7		-316.	279.	0.16	1
PK 98+ 4° 1			3	21259+5726	0.74		-290.	291.	0.03	1
PK 65–27° 1	-126.00	3.00	2	21274+1156	0.019	0.68				5
PK 89– 5° 1	-11.00	306.00	2	21306+4422	4.6	1.62				5
PK 86– 8° 1	24.00	336.00	2	21311+3924	0.39	0.12				5
PK 104+ 0° 1			3	22184+5759	0.76		-316.	279.	0.08	1
PK 100– 5° 1	-86.00	48.00	2	22219+5042	0.34	0.75				5
PK 100– 8° 1	-141.00	54.00	2	22296+4732	0.41	0.82				5
PK 107+ 2° 1	-31.00	579.00	1	22384+6101	4.1	0.75				5
PK 106–17° 1	-5.00	631.00	2	23234+4215	3.4	0.58				5
PK 111– 2° 1	5.00	600.00	1	23239+5754	7.5	1.34				5

Notes to Table C2:

References on the PN data:

1: Pottasch, 1984; 2: Zijlstra et al., 1989; 3: Acker, 1983;
4: Ratag et al., 1988; 5: Pottasch et al., 1988

References on the OH data:

1: Nançay: Te Lintel Hekkert et al., 1988d; 2: Parkes: Te Lintel Hekkert et al., 1988b;
3: Arecibo: Ederet al., 1988; 4: Dwingeloo: Te Lintel Hekkert et al., 1988b
5: Greenbank: Payne et al., 1988

Table C3. OH observations of Planetary Nebulae: possible detections

Name	Vel.$_{PN}$ PN [km s^{-1}]	6 cm flux density [mJy]	Ref. PN	IRAS name	F_{IR}^{tot} $\times 10^{12}$ [W m^{-2}]	IRE	peak velocity [km s^{-1}]		OH_{1612} flux [Jy]		Ref. OH
PK 311– 2° 1			3	14079–6402	1.3		29.5	44.9	0.28	0.32	2
PK 327– 2° 1	–72.00		3	15559–5546	3.9		1.3	–25.3	1.66	1.62	2
PK 352+ 3° 1			3	17087–3230	0.63		–63.9	–80.6	0.53	0.22	2
PK 352+ 3° 2			3	17115–3322	22.		–65.0	–73.4	1.26	0.97	1
PK 355+ 2° 1			3	17207–3059	0.11		2.9	20.4	0.14	0.19	2
							–60.2	–87.8	0.16	0.16	2
PK 358+ 3° 3		13	2	17253–2824	0.98	7.7	–13.9		0.26		2
							–117.9	–126.6	0.17	0.17	2
							–37.9	–49.0	0.13	0.51	2
							–70.3		0.16		2
PK 358+ 3° 1		47	2	17253–2824	0.37	0.88	–13.9		0.26		2
							–117.9	–126.6	0.17	0.17	2
							–37.9	–49.0	0.13	0.51	2
							–70.3		0.16		2
PK 355– 0° 1			3	17331–3324	0.62		–2.4	–6.1	6.67	1.42	2
							23.2	–25.0	3.48	7.97	2
PK 1+ 1° 1		32.30	2	17374–2700	0.64	2.11	63.8	82.1	0.22	0.11	2
PK 5+ 4° 2			3	17385–2211	0.34		16.3	35.6	0.16	0.18	1
PK 6+ 4° 1	–104.00	11	2	17403–2107	1.6		44.8		0.19		2
PK 0– 0° 1			3	17439–2845	72.		–325.7	–355.2	3.63	4.10	1
PK 0– 2° 1			3	17528–2910	0.088		106.2	134.4	0.52	0.33	2
PK 1– 3° 1	135.00	10	2	17574–2921	0.46	5.0	–83.8	–113.6	0.36	0.45	2
PK 8– 7° 2	205.00	98	0.85	18295–2510	0.76		67.6		0.39		2
PK 23– 1° 1			3	18376–0846	1.3		114.9	146.7	0.59	0.49	1
PK 45– 1° 1			3	19200+1035	0.86						3
PK 37– 6° 1	60.00	240.00	1	19204+0124	4.0	1.79	101.9	141.4	0.06	0.06	1
PK 56+ 2° 1			3	19255+2123	3.2		8.9	18.6	2.28	0.36	1
PK 59– 1° 2			2	19467+2213	0.51		–44.5	–16.3	0.15	0.03	3
PK 78+ 0° 1			3	20275+4001	310.		0.3	19.0	–0.19	0.22	4

Notes to Table C3:

References on the PN data:

1: Pottasch, 1984; 2: Zijlstra et al., 1989; 3: Acker, 1983;
4: Ratag et al., 1988; 5: Pottasch et al., 1988

References on the OH data:

1: Nançay: Te Lintel Hekkert et al., 1988d;
2: Parkes: Te Lintel Hekkert et al., 1988b;
3: Arecibo: Ederet al., 1988;
4: Dwingeloo: Te Lintel Hekkert et al., 1988b

References

Acker, A. 1983, *Astron. Astrophys., Suppl. Ser.* **54**, 315 .
Acker, A., Chopinet, M., Pottasch, S. R., Stenholm, B. 1987, *Astron. Astrophys., Suppl. Ser.* **71**, 163 .
Baud, B., Habing, H.J., Matthews, H.E., Winnberg, A. 1979a, *Astron. Astrophys., Suppl. Ser.* **35**, 179.
Baud, B., Habing, H.J., Matthews, H.E., Winnberg, A. 1979b, *Astron. Astrophys., Suppl. Ser.* **36**, 193.
Braun, R., Goss, W.M., Lyne, A.G. 1989, *Astrophys. J.*, in press.
Bedijn, P.J. 1987, *Astron. Astrophys.*, **186,** 136.
Bedijn, P.J. 1988, *Astron. Astrophys.*, **205,** 105.
Bowers, P.F. 1978, *Astron. Astrophys., Suppl. Ser.* **31**, 127.
Bowers, P.F., De Jong, T. 1983, *Astron. J.*, **88,** 655.
Burrabajal, V., Goméz-Gonzalez, J., Bachiller, R., Martín-Pintado, J. 1988, *Astron. Astrophys.*, **204,** 242.
Carter, J.C. 1986, Haystack Observatory Internal Report on "GLONASS Observations".
Caswell, J.L., Haynes, R.F. 1983a, *Aus. J. Phys.*, **36,** 361.
Caswell, J.L., Haynes, R.F. 1983b, *Aus. J. Phys.*, **36,** 417.

Caswell, J.L., Haynes, R.F., Goss, W.M., Mebold, U. 1981, *Aus. J. Phys.*, **34,** 333.
Chapman, J.M. 1988, *Monthly Notices Roy. Astron. Soc.*, **230,** 415.
Clegg, R., Walsh, J. R. 1989, in preparation.
Davis, L.E., Seaquist, E.R., Purton, C.R. 1979, *Astrophys. J.*, **230,** 434.
Eder, J., Lewis, B.M., Terzian, Y. 1988, *Astrophys. J. Suppl.*, **66,** 183.
Elitzur, M. 1982, *Rev. Modern Phys.*, **54,** 1225.
Engels, D., Schmid-Burgk, J., Walmsley, C.M., Winnberg, A. 1985, *Astron. Astrophys.*, **148,** 344.
Field, D. 1985, *Monthly Notices Roy. Astron. Soc.*, **217,** 1.
Fix, J.D., Mutel, R.L. 1984, *Astron. J.*, **89,** 406.
Gatley, I., Becklin, E. E., Werner, M. W. 1978, *Astrophys. J.*, **220,** 822
Genzel, R., Downes, D. 1977, *Astron. Astrophys., Suppl. Ser.* **30,** 145.
Habing, H.J., te Lintel Hekkert, P., Van der Veen, W.E.C.J. 1988, in IAU Symposium 131: Planetary Nebulae (Mexico City, october 1987), ed. S. Torres–Peimbert, in press.
Harvey, P. M. , Forveille T. 1988, *Astron. Astrophys.*, **197,** L19.
Herman, J., Baud, B., Habing, H.J., Winnberg, A. 1985, *Astron. Astrophys.*, **143,** 122.
Herman, J., Habing, H.J. 1985, *Physics Report* **124**, 255.
Iben Jr., I., Renzini, A. 1983, *Ann. Rev. Astron. Astrophys.*, **21,** 271.
Jones, T.J. 1986, in "Late Stages of Stellar Evolution", eds. S. Kwok and S.R. Pottasch (Reidel, Dordrecht), p 1.
Jura, M. 1986, *Astrophys. J.*, **309,** 732.
Kippenhahn, R. 1981, *Astron. Astrophys.*, **102,** 293.
Knapp, G.R. 1988, in IAU Symposium 131: Planetary Nebulae (Mexico City, october 1987), ed. S. Torres–Peimbert, in press.
Kerr, F.J., Bowers, P.F. 1974, *Astron. Astrophys.*, **36,** 225.
Kwok, S. 1985, *Astron. J.*, **90,** 49.
Kwok, S. 1986, in "Late Stages of Stellar Evolution", eds. S. Kwok and S.R. Pottasch (Reidel, Dordrecht), p 321.
Leene, A., Pottasch, S.R. 1987, *Astron. Astrophys.*, **173,** 145.
Likkel, L., Omont, A., Morris, M., Forveille, T. 1987, *Astron. Astrophys.*, **173,** L11.
Likkel, L., Morris, M. 1988, *Astrophys. J.*, **329,** 914.
te Lintel Hekkert, P., Habing, H.J., Caswell, J.L., Norris, R.P., Haynes, R.F. 1988, *Astron. Astrophys.*, **202,** L19.
te Lintel Hekkert, P., Versteege, H., Habing, H.J., Wiertz, M., 1989a, submitted to *Astron. Astrophys., Suppl. Ser.* (The OH/IR Catalogue)
te Lintel Hekkert, P., Caswell, J.L., Habing, H.J., Norris, R.P., Haynes, R.F. 1989b, in preparation.
te Lintel Hekkert, P., Le Squeren, A.–M., Habing, H.J., Sivagnanam, P., 1989c, in preparation.
Mauersberger, R., Henkel, C., Wilson, T. L., Olano, C. A. 1988, *Astron. Astrophys.*, **206,** L19
Morris, M., Guilloteau, S., Lucas, R., Omont, A. 1987, *Astrophys. J.*, **321,** 888.
Nedoluha, G. E., Watson, W. E. 1988, *Astrophys. J.*, **335,** L19
Olnon, F.M., Walterbos, R.A.M., Habing, H.J., Matthews, H.E., Winnberg A., Brzezinska, H., Baud, B. 1984, *Astrophys. J.*, **245,** L103.
Parthasarthy, M., Pottasch, S.R. 1986, *Astron. Astrophys.*, **154,** L16.
Payne, H.E., Phillips, J.A., Terzian, Y. 1988, *Astrophys. J.*, **326,** 368.
Phillips, J. P., Mampaso, A. 1988, *Astron. Astrophys.*, **190,** 237.
Pottasch, S.R. 1984, Planetary Nebulae (Reidel, Dordrecht). (P84)
Pottasch, S.R., Bignell, C., Zijlstra, A.A. 1987, *Astron. Astrophys.*, **177,** L49.
Pottasch, S.R., Bignell, C., Zijlstra, A.A., Olling, R. 1988, *Astron. Astrophys.*, **205,** 248.
Ratag, M., Pottasch, S.R., Zijlstra, A.A. 1989, in preparation.
Reid, M.J., Moran, J.M. 1981, *Ann. Rev. Astron. Astrophys.*, **19,** 231.
Rodriguez, L.F., Gomez, Y., Garcia-Barreto, J.A. 1985a, *Rev. Mexicana Astron. Astrof.* , **11,** 139.
Rodriguez, L. F., Garcia-Barreto, J. A., Cantó, J., Moreno, M. A., Torres-Peimbert, S., Costero, R., Serrano, A., Moran, J., Garay, G. 1985b, *Monthly Notices Roy. Astron. Soc.*, **215,** 353.
Rodriguez, L.F. 1987, *Planetary and Proto-Planetary Nebulae: From IRAS to ISO, Editor Preite Martinez*, p55 (Reidel Dordrecht).
Rowan–Robinson, M., Lock, T.D., Walker, D.W., Harris, S. 1986, *Monthly Notices Roy. Astron. Soc.*, **222,** 273.
Seaquist, E.R.,Davis, L.E. 1983, *Astrophys. J.*, **274,** 659.
Spergel, D.N., Giuliani Jr., J.C., Knapp, G.R. 1983, *Astrophys. J.*, **275,** 330.
Sun, J., Kwok, S. 1987, *Astron. Astrophys.*, **185,** 285.
Turner, B.E. 1970, *J. R. Astron. Soc. Can.* **64**, 221.
Turner, B.E. 1973, *Astrophys. J.*, **186,** 357.
van der Veen, W.E.C.J. 1988, PhD Thesis, University of Leiden.
Waelkens, C., Waters, L.B.F.M., Casatella, A., Le Bertre, T., Lamers, H.J.G.L.M. 1987, *Astron. Astrophys.*, **181,** L5.
Willems, F.J., de Jong, T. 1988, *Astron. Astrophys.*, **196,** 173.
Winnberg, A., Terzides, C., Matthews, H.E. 1984, *Astron. J.*, **86,** 410.
Zanstra, H. 1931, *Publ. Dom. Astroph. Obs.*,**4**, 209.
Zijlstra, A.A., Pottasch, S.R. 1988, *Astron. Astrophys.*, **196,** L9.
Zijlstra, A.A., Pottasch, S.R., Bignell, C. 1989, submitted to *Astron. Astrophys., Suppl. Ser.*
Zuckerman, B., Aller, L. H. 1986, *Astrophys. J.*, **301,** 772

This article was processed by the author using Springer-Verlag TEX AA macro package 1989.

Note added in proof: Recent VLA observations failed to detect OH emission from OHPN 3 and 4. These singledish detections may have been spurious. OH emission was confirmed from OHPN 5, 7, and 10, while for OHPN 6 and 11 the position of the OH emission is near, but possibly not identical to, the continuum source. OHPN 8 was not observed. The number of confused sources appears to be consistent with the expected confusion level, derived in Section 3.